REPORT DOCUMENTATION PAGE

Form Approved OMB No. 0704-0188

1. REPORT DATE *(DD-MM-YYYY)*	2. REPORT TYPE	3. DATES COVERED *(From – To)*
18-10-2004	Final Report	19 September 2001 - 19-Sep-03

4. TITLE AND SUBTITLE

Hybrid Fiber-Bulk Pulsed Erbium Laser

5a. CONTRACT NUMBER
F61775-01-C0008

5b. GRANT NUMBER

5c. PROGRAM ELEMENT NUMBER

6. AUTHOR(S)

Dr. William A Clarkson

5d. PROJECT NUMBER

5d. TASK NUMBER

5e. WORK UNIT NUMBER

7. PERFORMING ORGANIZATION NAME(S) AND ADDRESS(ES)

University of Southampton
Southampton SO17 1BJ
United Kingdom

8. PERFORMING ORGANIZATION REPORT NUMBER

N/A

9. SPONSORING/MONITORING AGENCY NAME(S) AND ADDRESS(ES)

EOARD
PSC 802 BOX 14
FPO 09499-0014

10. SPONSOR/MONITOR'S ACRONYM(S)

11. SPONSOR/MONITOR'S REPORT NUMBER(S)
SPC 01-4068

12. DISTRIBUTION/AVAILABILITY STATEMENT

Approved for public release; distribution is unlimited.

13. SUPPLEMENTARY NOTES

14. ABSTRACT

This report results from a contract tasking University of Southampton as follows: The contractor will investigate the development of a novel, eye-safe 1.6 micrometer laser source pumped by a high-power fiber laser co-doped with Erbium and Ytterbium, to produce a highly efficient, eye-safe source for use in laser radars, and atmospheric and environmental monitoring.

15. SUBJECT TERMS

EOARD, Lasers, Fibre Lasers, Eye-safe lasers

16. SECURITY CLASSIFICATION OF:			17. LIMITATION OF ABSTRACT	18, NUMBER OF PAGES	19a. NAME OF RESPONSIBLE PERSON
a. REPORT	b. ABSTRACT	c. THIS PAGE			DONALD J SMITH
UNCLAS	UNCLAS	UNCLAS	UL	61	19b. TELEPHONE NUMBER *(Include area code)* +44 (0)20 7514 4953

EOARD Project SPC 01-4068:
Contract order number: F61775-01-C0008

Hybrid Fiber-Bulk Pulsed Erbium Laser

Final Report

W. A. Clarkson, P. J. Jander, M. L. R. Laroche and J. K. Sahu

Optoelectronics Research Centre
University of Southampton
Southampton, SO17 1BJ
United Kingdom

Contents:

1.0 INTRODUCTION

The standard approach for producing laser output in the 1.5-1.6 micron wavelength region is via diode pumping of erbium-ytterbium co-doped bulk glass or crystal lasers. However, due to the short wavelength of the diode pump source (typically ~980nm) compared to the lasing wavelength, these lasers suffer from the problem that large fraction of the pump power is converted to heat in the bulk laser material. This leads to strong thermal lensing, which can severely degrade laser beam quality and efficiency, and thermally-induced stresses, which can cause catastrophic failure of the bulk material. A further problem is that due to the poor beam quality of the diode pump source it is necessary to use bulk material with relatively high Er and Yb concentrations. This has the effect of increasing energy-transfer-upconversion, which leads to increased thermal loading and a reduced energy storage time with the result that the laser efficiency is reduced. This problem is especially pronounced when operating the laser in Q-switched (pulsed) modes due to the higher excitation densities and can lead to a very significant reduction in the laser pulse energy.

An alternative approach for producing laser emission in the 1.5-1.6μm eyesafe wavelength regime is via cladding-pumping of a double-clad erbium-ytterbium co-doped fiber laser. Fiber lasers have recently attracted much interest due to their high efficiency, robustness, insensitivity to vibration and immunity to thermal effects, and are rapidly emerging as an attractive replacement to conventional bulk solid-state lasers for many applications requiring high-power cw output. However, due to their long device lengths and small core size, fiber lasers suffer from detrimental nonlinear effects, especially when operating in the high peak power pulsed regime, which can limit efficiency. Furthermore, pulse energies are generally limited by amplified spontaneous emission and/or parasitic lasing (due to their high gains) and ultimately by intensity-induced damage to the fiber end facets.

The main aim of this research program was to investigate an alternative strategy for producing high average power and high pulse energies in the ~1.6μm regime by employing a novel fiber-bulk hybrid laser scheme which combines the advantages of efficient cw high-power generation in cladding-pumped fiber lasers with the energy storage and high pulse energy capabilities of bulk solid-state laser crystals.

2.0 OBJECTIVES

The fiber-bulk hybrid laser scheme offers many potential advantages over laser systems based only on ‘bulk’ or fiber laser technology. The rationale behind the combination of fiber and bulk technologies in a hybrid laser system is as follows: Firstly, diode-pumping of an Er,Yb co-doped double-clad fiber laser allows the production of high-power cw output in the ~1.5μm wavelength regime suitable for direct ‘in-band’ pumping of a bulk Er-doped crystal. This has the important advantage over direct pumping of the bulk Er-doped crystal with a diode, that most of the heat generated via quantum defect heating (typically ~40%) is deposited in the fiber, with only ~6-7% of the fiber laser output power converted to heat in the bulk crystal. The net result is that thermal effects in the bulk Er laser are dramatically reduced leading to the prospect of much improved efficiency, beam quality and higher output power. The fiber laser benefits from a geometry that

allows relatively simple thermal management with the generated heat dissipated over a long device length (typically at least a few metres), thereby reducing the likelihood of thermally-induced damage. Furthermore, the output beam quality is determined by the waveguiding properties of the active-ion-doped core, which can easily be tailored to produce a single-spatial-mode output beam with little, if any, impact on beam quality due to thermal lensing.

Also, by employing an in-fiber Bragg grating or an external cavity with wavelength-dependent feedback provided by a simple diffraction grating, the Er,Yb fiber laser's wavelength can be tuned to precisely coincide with the strongest absorption line in the bulk Er material. This is facilitated in a glass host due to the very broad emission spectrum. The combination of good beam quality and wavelength tunability, provided by the fiber laser, also allows the use of long bulk crystals with low erbium concentrations. This reduces the deleterious effects of upconversion allowing long energy storage times and hence in principle high pulse energies can be achieved for relatively modest pump powers. The production of high pulse energies in the final bulk Er-doped crystal laser is further facilitated by the possibility of using much larger beam sizes than would be possible in the fiber laser, thereby reducing the risk of intensity-induced damage to the laser crystal or mirror coatings. Hence, the proposed hybrid laser scheme should allow efficient Q-switched operation in the required 1.6 micron spectral region with high output pulse energy and diffraction-limited beam quality, free from the problems of heat loading and/or reduced energy storage that currently limit the performance of conventional Er-doped bulk and fiber laser systems. A further attraction of the proposed scheme is that the final laser system can be extremely simple, robust and cost-effective.

The main objectives of this research program were as follows:

(a) To formulate a strategy for power scaling of cladding-pumped Er,Yb fiber lasers and to develop a high-power Er,Yb fiber laser with wavelength tunability from ~1.53-1.60 microns and with output power >10W.

(b) To investigate direct (in-band) pumping of an Er:YAG laser by the Er,Yb fiber laser to establish the design criteria for power scaling and for achieving high Q-switched pulse energies.

(c) To demonstrate a cw and Q-switched Er:YAG laser and evaluate the potential for scaling to higher powers and pulse energies.

3.0 POWER SCALING OF Er,Yb FIBER LASERS

3.1 Introduction

At the time this project commenced the maximum power demonstrated from a tunable Er,Yb fiber laser was ~6.7W at 1550nm and >4W over the wavelength range 1533nm to 1600nm [1,2]. This was achieved using a double-clad fiber with a phospho-silicate core of diameter, 12μm, and numerical aperture (NA), 0.175, and a pure silica inner-cladding of diameter, 125μm. The latter was surrounded by a low refractive index (n≈1.375) polymer outer-cladding to yield a high

numerical aperture of ~0.49 (calculated) for the inner-cladding pump guide. The fiber was pumped by beam-shaped output from a single diode-bar at ~915nm, and the overall optical-to-optical efficiency with respect to absorbed pump power was ~27% at 1550nm. Scaling the output power from the Er,Yb fiber laser to meet the requirements for efficient pumping of Er:YAG, whilst at the same time improving the efficiency, required a radical change in the fiber design and pumping architecture which proved to be somewhat more challenging to implement than first thought.

3.2 Diode-stack pump module and coupling scheme

Prior to the date this project commenced, cladding-pumped fiber lasers and amplifiers generally employed pump sources (e.g. fiber-coupled broad-area diodes and fiber-bundle-coupled diode-bars) of moderate power up to several tens-of-watts. Scaling such systems to higher power requires quite complicated (and expensive) pump multiplexing schemes. We therefore decided to investigate an alternative approach for power-scaling based on the use of diode-stacks. The rationale for this approach was that diode-stacks offer the higher output power of any commercially available diode (and are also the cheapest per watt). The net result is that fewer pump diodes and fewer optical components are required in the pump launching scheme thus reducing the overall complexity and cost. The main disadvantage of diode-stacks is the poor quality and unfriendly nature of their output beams. The beam propagation factor parallel to the diode array, M_x^2, is typically ~2000, and is many times larger than the beam propagation factor, M_y^2 (after fast axis collimation), in the stacking direction, making it difficult to focus to the small beam sizes required for efficient cladding pumping.

One solution to this problem is to re-shape the output beam so that $M_x^2 \approx M_y^2$, but without significantly degrading the brightness. Our approach is based on the use of a two-mirror beam-shaper [3]. This approach was developed in-house at the ORC several years ago and has been successfully applied to broad-area diodes and diode-bars to for efficient end-pumping of solid-state lasers and low-medium power double-clad fiber lasers. The principle of operation of the two-mirror beam-shaper is described in detail in ref.3. The basic idea (shown schematically in figure 1) is to use two high reflectivity mirrors to slice-up the combined output beam from the diode source in the x direction and stack the resulting beams in the orthogonal direction. As a rough guide, we can achieve a reduction in the value for M_x^2 to M_x^2/N and an increase in the value for M_y^2 to NM_y^2, where N is the number of times the incident beam is sliced. N is

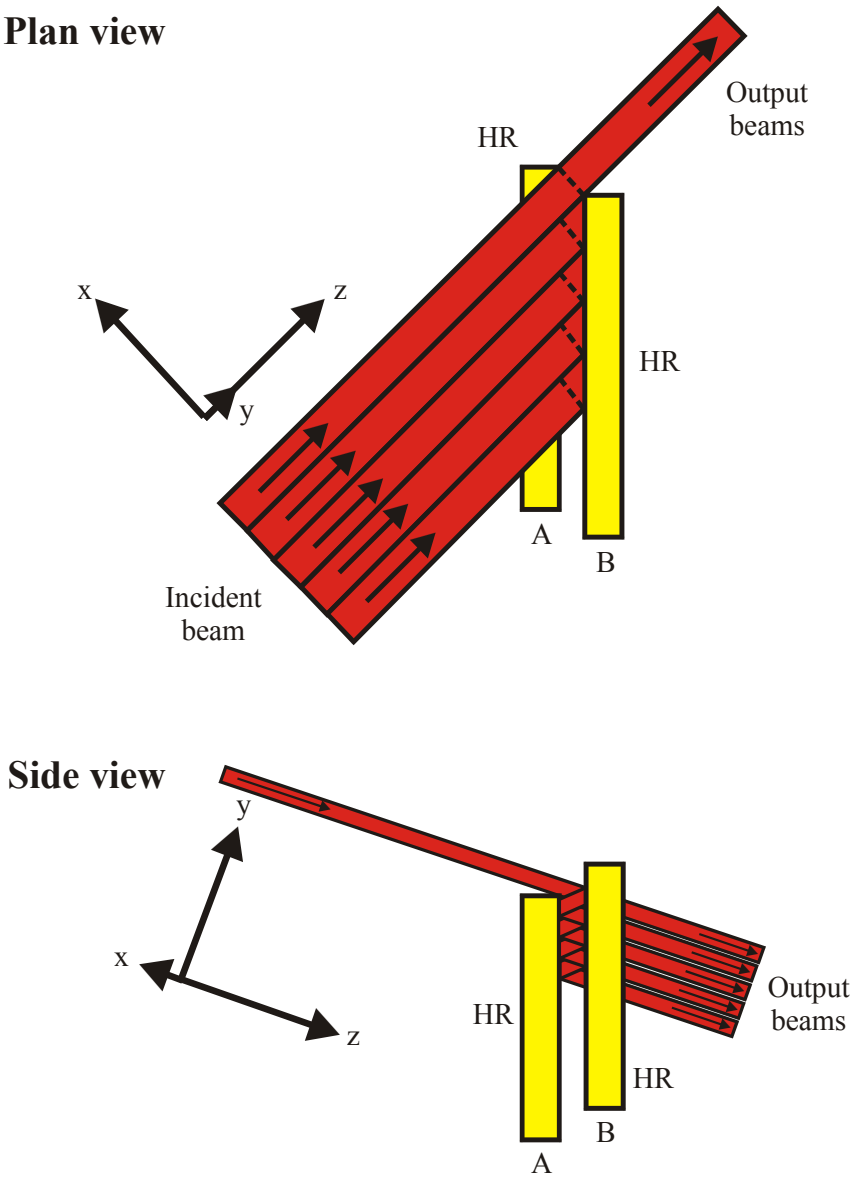

Figure 1: Two-mirror beam-shaper

normally selected (e.g. by adjusting the mirror separation and/or orientation, and/or the incident beam size) so that the emerging beam has roughly equal M^2 values in orthogonal planes. In practice, there is a small reduction in brightness due to leakage through the mirrors and because M_y^2 after beam shaping is $>NM_y^2$, since it is necessary to separate the stacked beams in the y-direction by a greater distance than the incident beam height to avoid loss due to clipping at the entrance aperture of the beam shaper. Further reduction in brightness can be avoided, or

minimized, by careful design and alignment of the beam shaper, and careful selection of the incident beam dimensions. The key attractions of this approach are low loss and simplicity, since only two relatively standard components (i.e. mirrors) are required for beam shaping. Obviously, further complexity is added due to the need for a combination of cylindrical and spherical lenses for conditioning of the output beam from the diode laser to match the requirements for beam shaping and, also, for re-collimating and focusing of the re-shaped output beam.

We have applied this approach to two 160W cw (4-bar) stacks operating at ~940nm (purchased from DILAS DiodenLaser GmbH) using the optical arrangement shown in figure 2. The output from each bar on the stack was first collimated by a high numerical aperture cylindrical microlens (FAC-850 from LIMO GmbH), and then imaged on to the entrance aperture of the two mirror beam-shaper via an arrangement of crossed cylindrical lenses, f_1 and f_3, and f_2 and f_4 respectively. The lenses were selected to produce a highly elliptical beam with $w_x >> w_y$,, where w_x and w_y are the beam widths in the x and y directions respectively. It is important that the beam width in the y direction is not too small, so that the Rayleigh range, $z_{oy} > w_x$, otherwise there is significant diffraction spreading of the beams in the y-direction as they pass through the beam shaper, leading to a reduction in brightness. Based on the diode-stack specifications available from the manufacturer we estimate that initial beam propagation factors (i.e. before beam shaping) were $M_x^2 \sim 2000$ and $M_y^2 \sim 14$ (after collimation by the microlens array). The latter value takes into account the likelihood that there will be some degradation in the beam quality for each diode-bar during collimation due to lens aberrations and misalignment. It should be stressed that accurate alignment of the microlenses is crucial for good performance of the whole focusing system. Our aim was to configure the beam shaper to produce a re-shaped beam with beam quality factors in orthogonal planes $M_{xf}^2 \approx M_{yf}^2 \approx (1.3 M_x^2 M_y^2)^{1/2} = 190$ by slicing the input beam ~11 times. The factor of 1.3 is to allow for extra spacing between stacked beams in the y direction to minimize loss due to clipping on the first beam-shaper mirror. To achieve this, focal lengths, f_1=38mm, f_2=200mm, f_3=150mm and f_4=40mm, were selected to produce a beam of width ~40mm in the x direction and ~1.2mm in the y-direction at the beam-shaper entrance aperture. The beam shaper mirror spacing and orientation were then adjusted to produce 11 stacked beams. We obtained 145W of output power from the beam shaper at the maximum drive current, which corresponds to 165W after collimation by the microlenses. This is a much higher transmission than is usually achieve with single bars or broad-area diodes due to the 'top-hat' intensity profile of the beam in the y direction.

The output from the beam-shaper was re-collimated in the x direction by a cylindrical lens of focal length 300mm and then focussed by a Gradium lens of focal length 20mm. At the waist we measured beam radii of 162μm and 398μm in the x and y directions respectively. The values for M_{xf}^2 and M_{yf}^2 were determined using a scanning slit to measure the beam size versus position. We found that $M_{xf}^2 \approx 100$ and hence was somewhat smaller than expected. Unfortunately, M_{yf}^2 was much larger than expected with a value of approximately 360. This was attributed mainly to

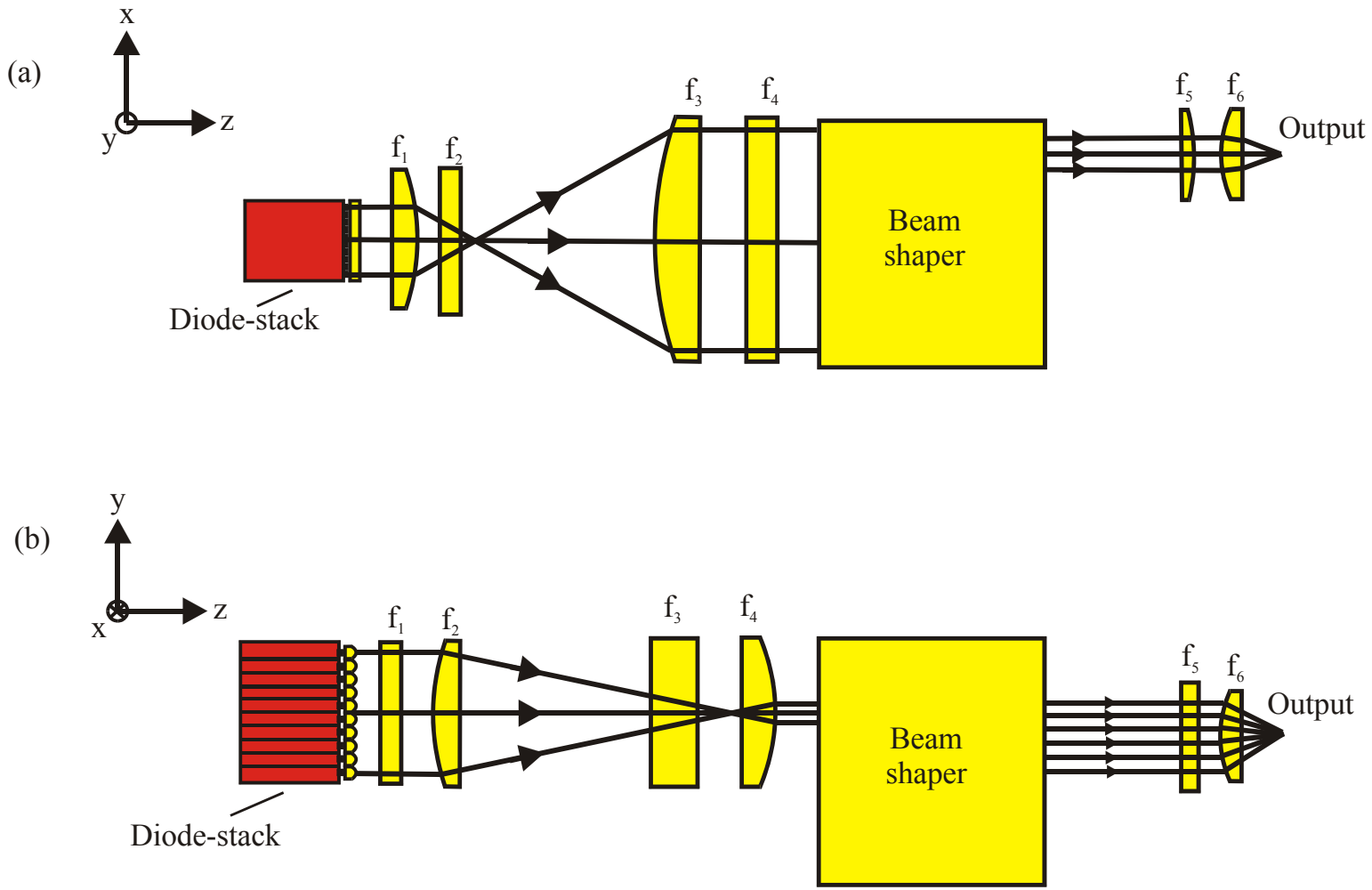

Figure 2: (a) Plan view and (b) side view of focusing scheme

inaccurate positioning of the fast-axis collimating lenses in the y and z directions (see Fig.1). The tolerance for positioning of these lenses relative to each other in the y direction, so that collimated beams propagate parallel to each other, is very tight and difficult to meet. As a very rough guide, the degradation in beam quality for the combined beam in the y direction will become significant when the angular misalignment, $\Delta\alpha$, of collimated beams from adjacent bars is comparable to the beam divergence, θ_B of an individual collimated beam. To avoid degradation beam quality requires $\Delta\alpha << \theta_B$, which in turn requires that the tolerance on positioning of the microlenses in the y direction for adjacent bars, $\Delta y << h_e$, where h_e is the beam size in the y direction at the diode-bar facet (typically ~1μm).

To improve the final beam quality, we have refined our procedures for aligning and fixing the microlenses in position. We are now able to position adjacent microlenses in the y direction to an accuracy of around ±0.5μm. There is still scope for further improvement, but this is probably the best that we can achieve for the time being. Further improvements in microlens positioning may, in any case, be offset by other sources of degradation in beam quality in the y direction (e.g. diode-array curvature ('smile'), and microlens quality).

The beam-shaped 160W cw (4-bar) diode-stack pump modules were re-assembled using to new microlens alignment procedure and tested. For the new set-up we obtained beam quality factors, $M_{xf}^2 \approx 133$ and $M_{yf}^2 \approx 270$, in the x and y directions respectively. A photograph of the beam-shaped diode-stack pump module is shown in figure 3. The minimum inner-cladding diameter, d

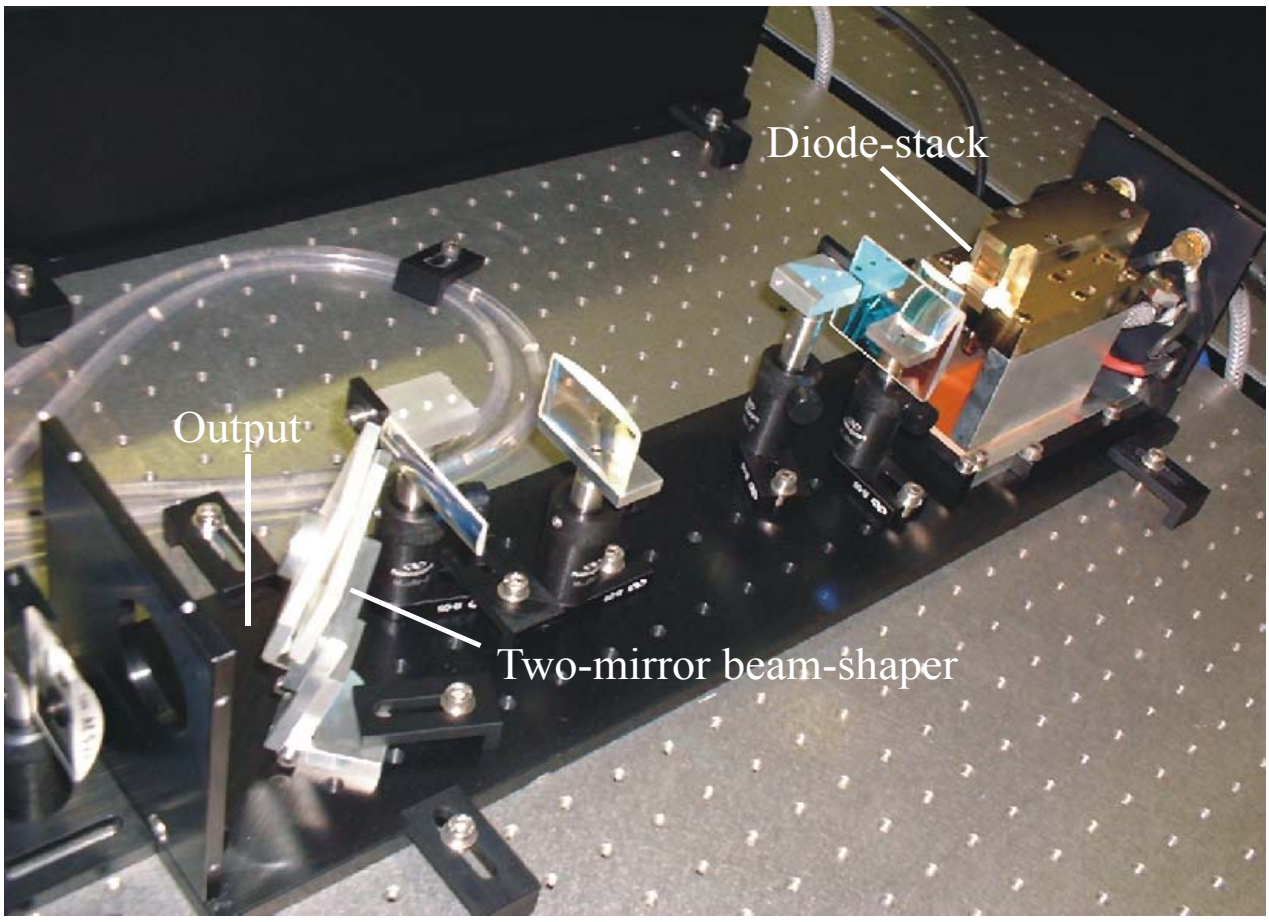

Figure 3: Beam-shaped diode-stack pump laser

required for efficient launching of the output from the pump module can be estimated from:

$$d = \frac{2\gamma_w \gamma_{na} M^2 \lambda_p}{\pi \theta_{na}} \quad (1)$$

where θ_{na}=arcsin(NA), and γ_w and γ_{na} are the ratios by which the focussed beam size and far-field beam divergence should under fill the fiber inner-cladding diameter and θ_{na} for efficient in-coupling respectively. The values of γ_w and γ_{na} need to be selected to give a high launch efficiency, but without resulting in a significant degradation in the beam quality on launching into the fiber. If we choose $\gamma_w \approx \gamma_{na} \approx 1.2$ (to achieve high launch efficiency and minimise the risk of damage caused by un-coupled pump light), and the inner-cladding NA is 0.4, then the minimum inner-cladding dimensions required diameter required are ~290µm and 590µm for the x and y direction respectively. There is certainly scope for a further improvement in the output beam quality and hence brightness from the beam-shaped diode-stack, allowing coupling into smaller diameter fibers by improving the positioning accuracy of the fast-axis collimating lenses. Alternatively, the re-shaped output beam could be divided into two beams with $M_{yf}^2 \approx M_{xf}^2 \approx 135$ and the two beams could be polarisation-combined to produce a single beam with $M_{yf}^2 \approx M_{xf}^2 \approx 135$, which could be launched efficiently into a circular fiber with inner-cladding diameter of ~300µm. However, for simplicity and because the available pump far exceeded the requirements for power-scaling of the Er,Yb fiber, we employed the optical arrangement shown in figure 4, which employs a water-cooled copper aperture as a spatial filter to improve the beam quality factor in the y direction (at the expense of pump power) prior to focussing into the fiber. This has the advantage that a greater fraction of the pump light incident on the fiber can be launched, hence reducing the risk of damage. With this arrangement and a focussing lens of 25mm focal length ~73% of the pump light could be launched into a 400µm diameter fiber corresponding to a launched power of 45W.

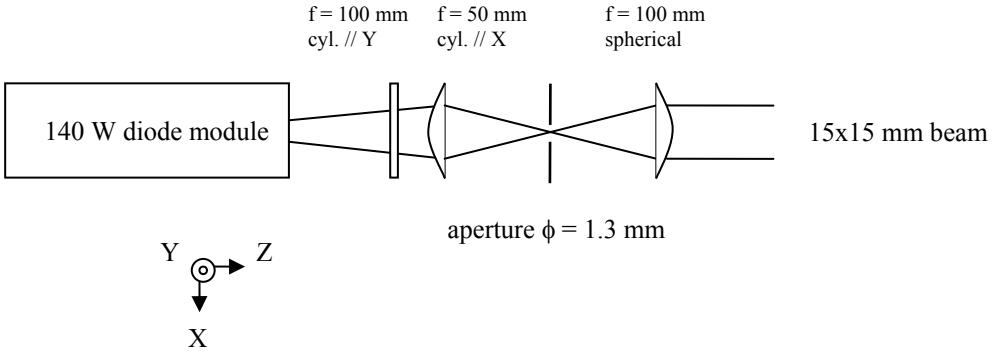

Figure 4: Beam conditioning arrangement for diode-stack module

3.3 Er,Yb fiber laser design

A detailed investigation of some of the main factors affecting the performance of Er,Yb co-doped double-clad phosphosilicate fiber lasers (EYDCFLs) was conducted to allow a design strategy for Er,Yb fiber to be formulated. Laser efficiencies can vary significantly with only small changes in the fiber design and fabrication procedure, so it is extremely important to identify the main factors affecting the overall efficiency. Er^{3+} and Yb^{3+} ion concentrations and background losses due to unwanted impurities are two parameters which can have a strong influence on laser performance. To gauge the importance of these factors a number of laser and spectroscopic measurements were performed on four EYDCFs fabricated from four performs with the same ratio of ion concentrations ($[Yb^{3+}]/[Er^{3+}]$~20), but different absolute concentrations.

(a) Comparison of laser performance

The experimental arrangement used to investigate laser performance (shown in figure 5) used a Ti:sapphire pump laser coupled into a multimode fiber to mimic the pump beam from a high power diode laser pump source. The fiber laser employed a very simple cavity configuration, with feedback for laser oscillation provided by a dichroic mirror (HR at 1.5-1.6μm and HT at 915-920nm) butted to one end of the fiber, and by the 3.6% Fresnel reflection from the cleaved facet at the other end of the fiber.

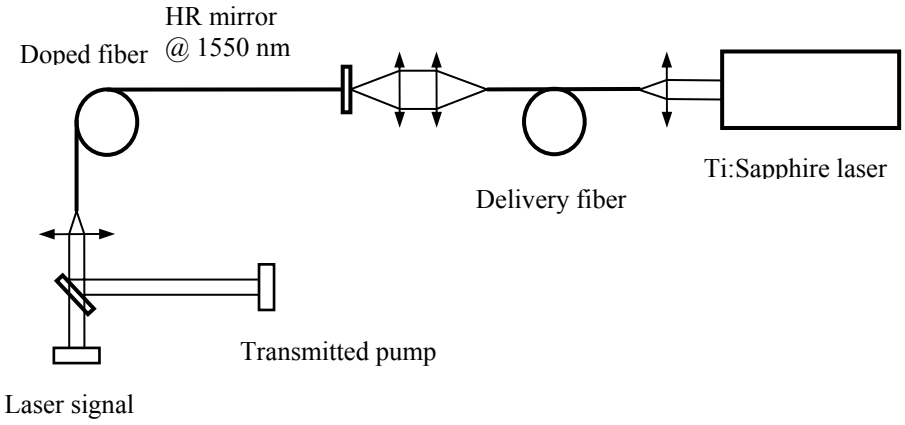

Figure 5: Experimental set-up for laser measurements

The details of the fibers and their slope efficiencies for different fiber lengths are summarised in table 1. It can be seen that the maximum slope efficiency varies significantly from fiber to fiber. The maximum slope efficiency (~46 %) was achieved for a fiber pulled from preform HD 643. This is quite close to the theoretical upper limit of 49% calculated from [4]:

$$\eta = \eta_p \cdot \left(\frac{1-R}{\left(1+\sqrt{R}\right)^2} \right) \cdot \left(\frac{4}{L - \ln R} \right) \qquad (2)$$

where $\eta_p \approx \lambda_{pump}/\lambda_{laser}$ is the maximum pumping quantum efficiency (~59% for a pump wavelength of 915nm and lasing wavelength of 1550nm), R is the reflectivity of the output facet and L the total round-trip loss (assumed to be negligible in this case). In contrast, the slope efficiencies for fibers pulled from performs; HD 653, HD 655 and HD 576 were much lower.

Preform Ref. No.	**Length** (cm)	**Cladding diameter** (μm)	**Core diameter** (μm)	**Cladding Losses @ 875 nm** (10^{-4} cm^{-1})	N_T (Yb^{3+}) (10^{-20} cm^{-3})	**Slope Efficiency** (%)	**Threshold** (mW)
HD 643	167.5	125	11.2	9.57	10.16	33.6	190
	127.5					38.7	151
	107.5					41.9	133
	87.5					45.6	113
	67.0					44.8	92
	47.0					43.2	82
	27.0					26.3	63
HD 653	203.0	125	14.8	10.79	4.28	23.0	169
	169.0					25.9	167
	139.0					24.5	162
	136.0					25.6	128
	116.0					27.0	130
	96.0					28.8	118
	69.0					29.1	86
	49.0					28.3	62
HD 655	103	125	11	-	7.41	23.9	99
	73					34.7	79
	52					31.7	54
HD 576	310	125	14.4	-	1.44	23.4	148
	221					27.4	96
	85					24.7	34

Table 1: Properties and laser performance of the studied fibers

A number of experiments were conducted with the aim of identifying the reason(s) for the difference in slope efficiencies. There are a number of factors that can affect the maximum slope efficiency including inner-cladding/core propagation losses, and Er^{3+} and Yb^{3+} ion concentrations.

The inner-cladding propagation losses were measured for two fibers with markedly different slope efficiencies by simply tuning the Ti:sapphire to a wavelength ~875nm, where there is negligible absorption by the Yb and Er dopants. Both fibers were found to have cladding propagation losses of approximately 0.44dB/m. This is somewhat higher than expected, but would not have a significant impact on the slope efficiency for the short fiber lengths used in this study.

The core propagation loss as a function of wavelength was measured by coupling white light into the doped fiber and analysing the transmitted light with an optical spectrum analyser for different

fiber lengths. To prevent light from propagating in the inner-cladding (which would give misleading results), it was necessary to splice a short length of standard single-mode fiber on to the double-clad Er,Yb-doped fiber. The resulting measured values for core propagation loss at wavelengths of 700 and 1200nm are given in table 2.

Fiber	Losses @ 700 nm (dB/m)	Losses @ 1200 nm (dB/m)
HD 643	0.186	0.505
HD 653	1.503	2.78
HD 655	1.88	2.68
HD 576	< 0.1	< 0.1

Table 2: Measured propagation losses into the fiber core

Fibers from preforms HD-653 and HD-655 have rather high core propagation losses (>1.5dB/m), which helps to explain why their slope efficiencies are low compared to the fiber from HD 643. It is worth noting that the core losses are much higher at 1200 nm, which is rather unusual and is thought to be due to contamination by other metal ions. The core losses were not measured around 1550 nm because of the high erbium absorption between 1400nm and 1700 nm. Further evidence supporting the high core propagation losses for fibers from HD 653 and HD 655, is the increase in slope efficiency for shorter fiber lengths (see Table 1).

One interesting observation was that the fiber from HD 576 also has a very low slope efficiency (<28%) in spite of the fact that it has low propagation losses. This is strong evidence for the important role played by the ion concentrations in determining the overall efficiency, since this fiber has much lower Er^{3+} and Yb^{3+} concentrations than the fiber from HD 643. In fact, it can be seen from Table 1 that that there is a strong correlation between Yb^{3+} (and therefore Er^{3+}) concentration and slope efficiency. Part of the reason for this is that a higher Yb concentration leads to a higher absorption coefficient for the pump and hence a shorter fiber with lower loss. However, this is not the whole story, since there are other factors (e.g. energy transfer efficiency) which impact on the slope efficiency and which also depend on the active ion concentrations.

(b) Spectroscopic measurements

To study the influence of Er and Yb concentrations on energy transfer efficiency we measured the fluorescence lifetimes of the emitting levels of erbium and ytterbium as a function of pump power for the different fibers using the experimental arrangement shown in figure 2. In this experiment, a simple chopper was used to modulate the pump and the fluorescence was collected from the side of the fiber to avoid re-absorption or amplified spontaneous emission influencing the results. The results of this investigation are summarised in the table 3. For each fiber, two values of the fluorescence lifetime are given corresponding to fluorescence collected from the beginning and end of the fiber respectively.

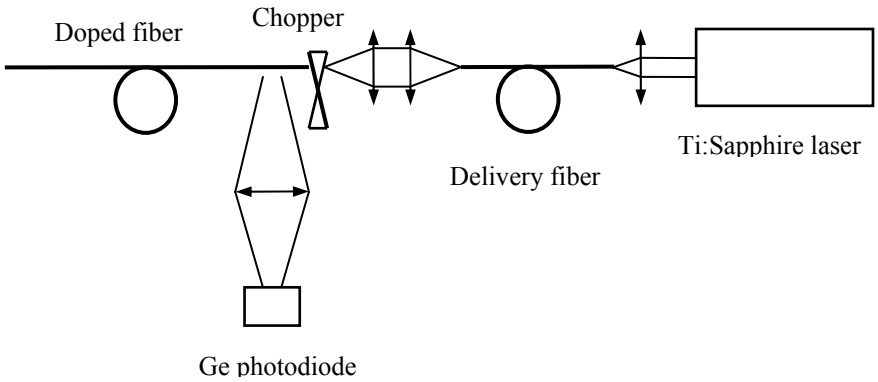

Figure 6: Experimental set-up for fluorescence measurements

In Yb-doped phospho-silicate fibers the upper laser level lifetime is ~1.3ms. However, in co-doped fibers, the energy transfer is usually very efficient with the result the Yb lifetime is dramatically reduced (to ~10μs) if no saturation occurs. One way to avoid energy transfer saturation is to use a low pump power to excite Yb^{3+} ions. However, at these low power levels it is difficult to detect the Yb^{3+} fluorescence, either because the power is too low or because the energy transfer to Er^{3+} is so efficient (i.e. the lifetime is very short). Since a shorter lifetime indicates a more efficient energy transfer, we can deduce that the HD-643 fiber has the most efficient energy transfer and the HD-576 fiber has the least efficient energy transfer. As a rough guide, the energy transfer efficiency η can be estimated from:

$$\eta = 1 - \frac{\tau_f}{\tau_0} \tag{3}$$

where τ_f is the fluorescence lifetime in the co-doped fiber and τ_0 is the fluorescence lifetime Yb-doped fiber.

Fiber	Length (cm)	Incident Power (mW)	Yb^{3+} Lifetime (μs)	Energy transfer efficiency (%)	Er^{3+} Lifetime (ms)
HD 643	48	610 80	440 - 481 -	63 - 66	9.05 – 9.1 9.0 – 9.1
HD 653	51	670 20	488 - 548 -	58 - 63	9.50 – 9.57 9.66 – 10.4
HD 655	27	670 20	536 - 585 -	55 - 59	9.11 - 9.29 9.72 – 9.74
HD 576	43	670 30 – 40	704 - 789 729	39 - 46	9.13 - 9.53 9.82 – 10.03

Table 3: Fluorescence lifetime and evaluation of energy transfer efficiency in phospho-silicate fibers

Energy transfer can be limited either by a strong saturation, which means the Er^{3+} concentration is too low to receive the energy stored by Yb^{3+} ions or by a low overall Er/Yb concentration. In our case these two factors are probably limiting the energy transfer since the Yb^{3+} lifetime increases with the pump power. Further evidence of energy transfer saturation has been obtained from a comparison of the fluorescence intensities for the Er^{3+} and Yb^{3+} ions versus pump power (as shown in figure 7). In all fibers we found a linear dependence of the Yb^{3+} fluorescence on pump power, and saturation of the Er^{3+} fluorescence (hence the $^4I_{13/2}$ Er^{3+} state population) at a pump power of a few hundreds of milliwatts. These results show that energy transfer saturation can be a serious problem, particularly when lasers are operated in pulsed (Q-switched) and/or with high resonator losses. Under these circumstances, a lower ratio of $[Yb^{3+}]/[Er^{3+}]$ should yield improved performance. However, under cw lasing conditions with low cavity losses, the Er^{3+} population inversion is clamped at a lower level, so energy transfer saturation should be negligible.

Loss due to upconversion from the emitting level $^4I_{13/2}$ in Er is also a potential mechanism for reduced lasing efficiency. In most of the fibers tested, the decrease in Er^{3+} fluorescence lifetime with increasing pump power (see Table 3) is evidence for upconversion. The decrease in efficiency which results from upconversion can be a serious problem, particularly for lasers operated in pulsed mode or with high cavity losses. In cw lasers with low cavity losses, the loss due to upconversion is clamped at threshold and hence should not have a significant impact on efficiency.

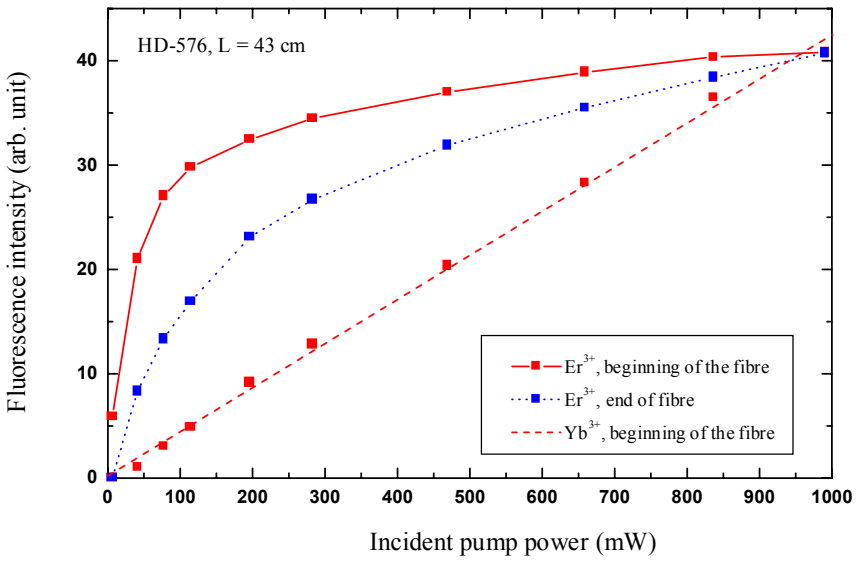

Figure 7: Comparison of the fluorescence intensity evolution for Yb^{3+} and Er^{3+} ions

The excitation spectrum of Yb^{3+} was also measured to see if the pump wavelength had an effect on the Er^{3+} population (figure 8). The fluorescence intensity follows the Yb^{3+} absorption quite well, except around the peak absorption at 970 nm. This is probably due to energy transfer saturation and/or pump ESA from $^4I_{11/2}$ state to $^4F_{7/2}$. One very interesting observation was that

the fluorescence intensity decreased quite dramatically (by up to 50%) at certain pump wavelengths. We are not sure of the explanation for this behaviour, but believe it may be due very narrow water absorption lines. If so, then it should not be a problem providing the diode pump wavelength can be temperature tuned to avoid these absorption lines.

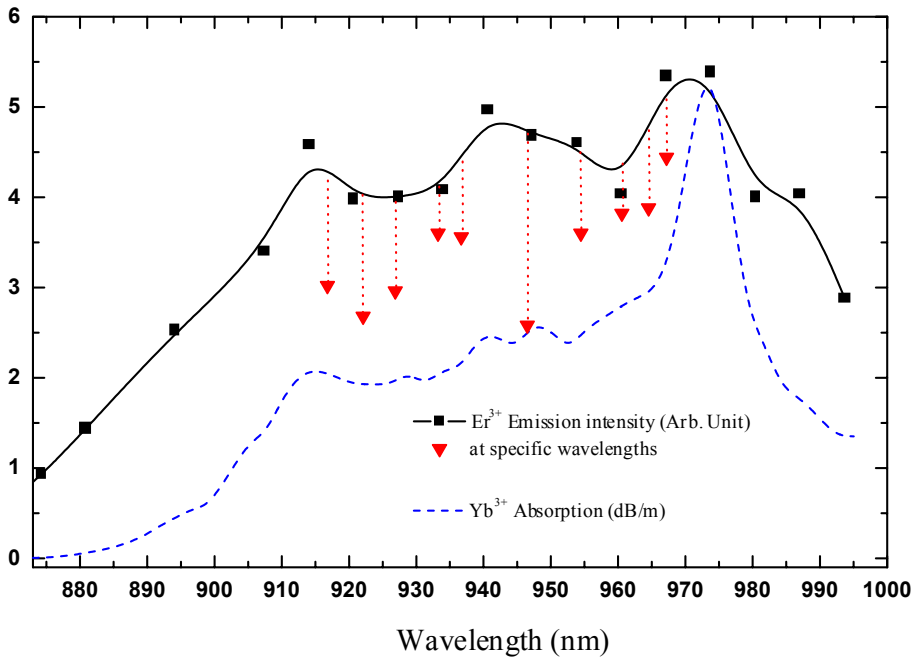

Figure 8: Excitation spectra of Yb^{3+} in phospho-silicate fiber by measuring Er^{3+} emission (P_{pump} = 40 mW)

(c) Analysis and modelling of the erbium-ytterbium phospho-silicate fiber

In order to get a better understanding of our experimental results and to formulate a strategy for optimising the design of our fibers, we have developed an approximate model for Er,Yb-doped phospho-silicate fibers taking into account a number of different processes which can affect lasing efficiency. The Er^{3+} ion is one of the most complicated rare-earth ions in terms of excited-state processes and so it is extremely difficult to make accurate predictions of its behaviour in a given host or for a given ion concentration. However, in the case of phospho-silicate fibers, the relatively high maximum phonon energy leads to a dramatic decrease in the lifetime of some energy levels so that some ESA transitions can be ignored and hence the problem can be greatly simplified. The spectroscopic processes considered in our model are illustrated in figures 9 and 10.

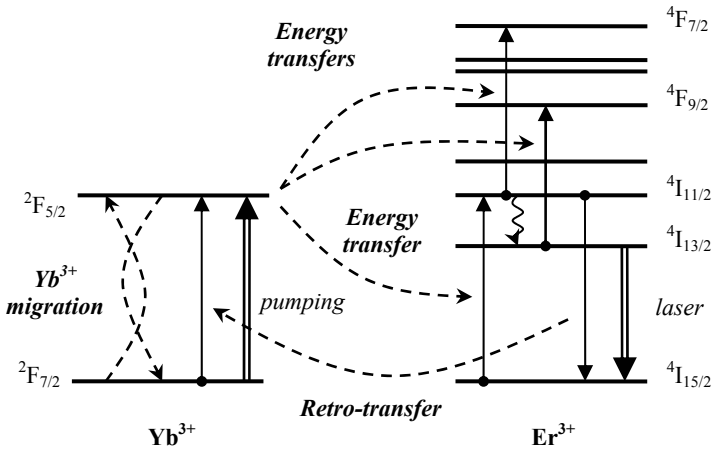

Figure 9: Er^{3+} - Yb^{3+} energy transfer mechanisms

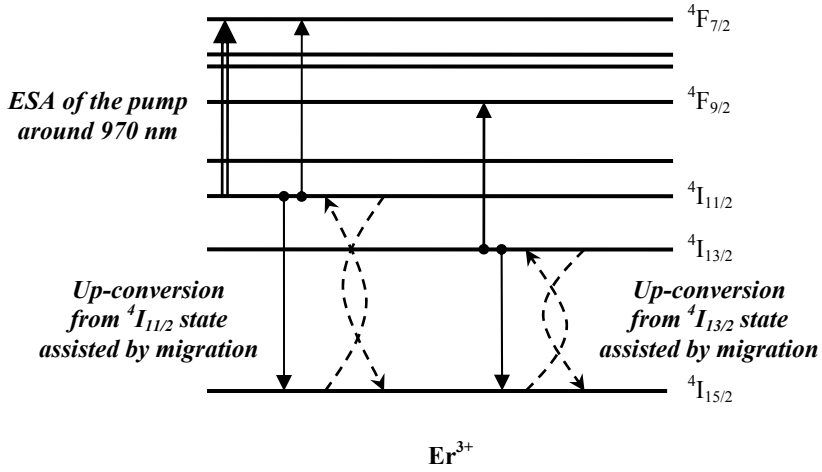

Figure 10: Potential loss mechanisms from $^4I_{11/2}$ and $^4I_{13/2}$ states of Er^{3+}

The lifetimes of the different energy levels were estimated using Judd-Ofelt analysis (for radiative lifetimes) and the gap law (for non-radiative transitions by phonon emission). In both calculations, we have assumed that the parameters relevant to the host were the same as for phosphate glass [5]. The results of the calculations (given in Table 4) show that the lifetime of the Er^{3+} emitting level is not affected by non-radiative de-excitation. The $^4I_{11/2}$ lifetime on the other hand is strongly quenched leading to a faster population of the Er emitting level and a reduction in loss due to ESA from this level.

Energy level	Radiative lifetime (ms)	Non-radiative lifetime (μs)	Fluorescence lifetime (μs)
$^4S_{3/2}$	0.68	0.267	0.267
$^4F_{9/2}$	0.80	0.104	0.104
$^4I_{9/2}$	6.78	$6.21\ 10^{-3}$	$6.21\ 10^{-3}$
$^4I_{11/2}$	6.42	3.981	3.981
$^4I_{13/2}$	7.80	$4.183\ 10^{6}$	7800

Table 4: Calculated radiative and non-radiative lifetimes

Our model is based on the population evolution equations, where Yb^{3+} is represented by two energy levels ($^2F_{7/2}$ and $^2F_{5/2}$) and Er^{3+} by five ($^4I_{15/2}$, $^4I_{13/2}$, $^4I_{11/2}$, $^4F_{9/2}$ and $^4F_{7/2}$). The macroscopic probabilities of the various processes (shown in figures 9 and 10) were calculated using Forster-Dexter theory [6] and the Inokuti and Hirayama model [7]. The effect of energy migration between two donor ions on probabilities was also taken into account using either the "hopping model" or the "diffusion model" as indicated in Table 5. The ESA spectra needed to evaluate the probabilities for energy transfer via upconversion and ESA were assumed to be similar to those reported for bulk phosphate glass [5].

Process	Model	Calculated macroscopic probability (10^{-16} cm^3.s^{-1})	Measured macroscopic probability (10^{-16} cm^3.s^{-1}) [Valley, 2001]
$Yb^{3+} \rightarrow Er^{3+}$ Energy transfer from $^4I_{15/2}$	Hopping-Model	1.54	1.0 – 5.0
$Yb^{3+} \rightarrow Er^{3+}$ Energy transfer from $^4I_{13/2}$	Hopping-Model	0.085	-
$Yb^{3+} \rightarrow Er^{3+}$ Energy transfer from $^4I_{11/2}$	Hopping-Model	1.42	-
$Er^{3+} \rightarrow Yb^{3+}$ retro-transfer	Diffusion Model	0.675	-
$^4I_{11/2}$ up-conversion	Diffusion Model	$5.17\ 10^{-38}$ cm^3 (by / N_{Er})	-
$^4I_{13/2}$ up-conversion	Hopping-Model	$5.75\ 10^{-3}$ $1.13\ 10^{-38}$ cm^3 (by / N_{Er})	$8.0 – 35.0\ 10^{-3}$

Table 5: Calculated macroscopic probabilities for energy transfer and up-conversion processes

The first stage was to evaluate the importance of each loss process by calculating the fraction of photons lost versus pump energy due to each process in a pumped Er,Yb fiber without feedback. Figure 11 shows that the dominant loss processes for fiber HD643 is predicted to be inefficient energy transfer from Yb^{3+} to Er^{3+}. The low energy transfer efficiency is due to a high Er^{3+} population inversion. Once again, it should be stressed that under cw lasing conditions the $^4I_{13/2}$ population would be much lower and hence energy transfer from Yb^{3+} should not be a cause of low lasing efficiency. There are other processes (not shown in figure 11) which might decrease efficiency, for example, pump ESA from $^4I_{11/2}$ and signal ESA from $^4I_{13/2}$, but these processes are only likely to be a problem for a pump wavelength around 970nm and for a signal wavelength >1600nm respectively.

Figure 12 shows the calculated Er^{3+} and Yb^{3+} emitting level populations and the stored energy in Er^{3+} versus pump energy for fiber HD 643. It can be seen that the $^4I_{13/2}$ population reaches a maximum after only 600 μs (for 1W of incident pump power), which is interesting from the point of view of Q-switched operation. Indeed, because of the fast saturation of the energy transfer and the short lifetime of Yb^{3+}, this fiber cannot store much energy.

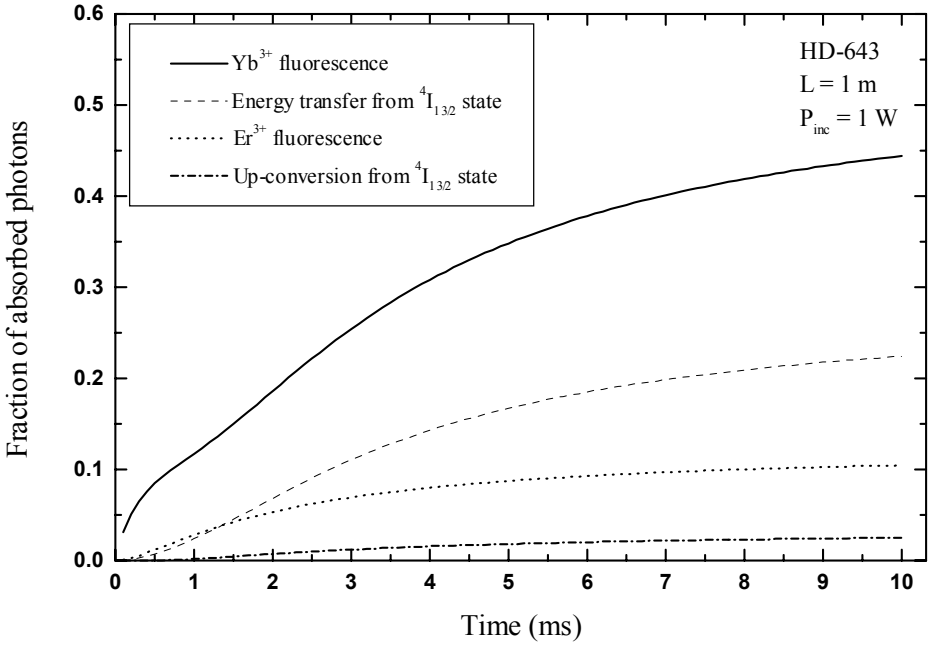

Figure 11: Calculated losses by ESA or fluorescence processes in Er/Yb fiber

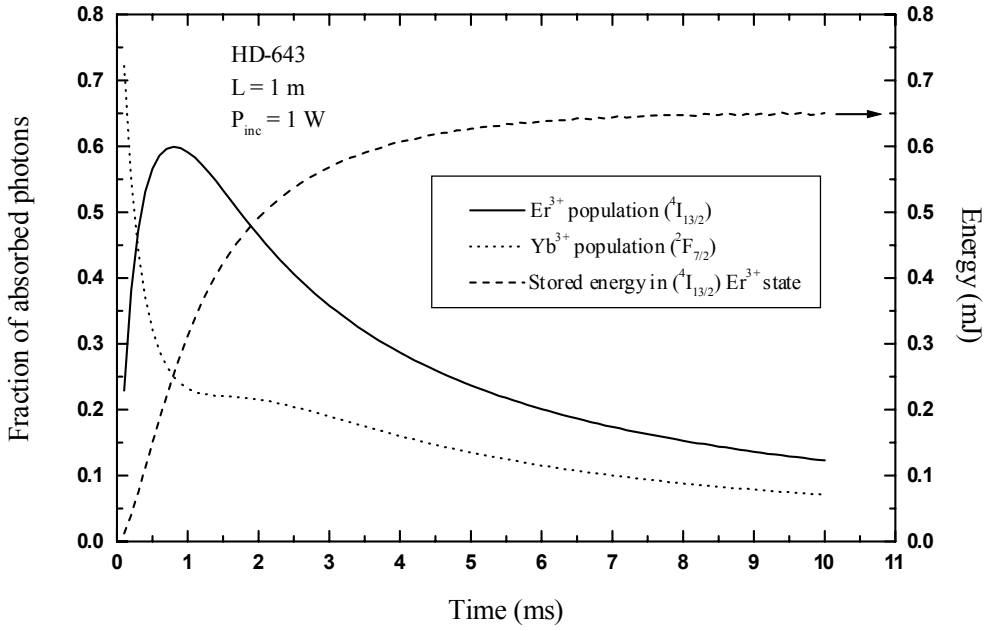

Figure 12: Calculated Er^{3+} and Yb^{3+} emitting levels population relative to the absorbed pump photons and stored energy by Er^{3+}.

Cw laser operation of each fiber was simulated for the length of fiber which gave the best slope efficiency. Propagation losses in the cladding (0.5dB/m) and the core (see Table 2) were taken into account and the resulting predicted values for slope efficiency compared with the measured values in Table 6.

Fiber	Length (cm)	Measured Slope efficiency (%)	Calculated Slope efficiency (%)
HD 643	87.5	45.6	41.0
HD 653	69.0	29.1	18.0
HD 655	73.0	34.7	28.1
HD 576	221.0	27.4	4.0

Table 6: Comparison between measured and calculated laser slope efficiencies

It is worth noting that the predicted values for slope efficiency are somewhat lower than the measured values, which we believe may be due to an under estimate of the energy transfer parameters (especially for fiber HD576). However, the trend is correctly simulated by the model. In order to determine the optimum concentration ratio of Yb^{3+} to Er^{3+}, slope efficiencies were calculated for different concentration ratios R (keeping the Yb^{3+} concentration constant) for the HD-643 fiber (without core losses) and for the HD-655 fiber with core losses of 1.88 dB/m. The results are presented in Table 7, and suggest that the optimum value for the concentration

ratio is between 2 and 5. In practice, this would probably be achieved by increasing the Er^{3+} concentration with the result that it would be more difficult to achieve a high population inversion and may result in a decrease in gain and a decrease in the wavelength tuning range. To test these predictions, double-clad Er/Yb fibers with a range of concentration ratios from R=20 to R=5 and with core/cladding diameters suitable for cladding-pumping were fabricated and tested at high pump powers. The results of this study are described in section 3.5.

R	HD-643	HD-655
2	44.0	41.9
5	51.0	40.0
10	45.3	36.4
15	44.6	32.1
20	41.3	28.1
25	38.1	25.7

Table 7: Slope efficiency calculated for different values of the Yb/Er concentration ratio

3.4 Passively Q-switched Er,Yb fiber laser

Passive Q-switching of a cladding-pumped Er,Yb fiber laser using Co^{2+}:ZnS as the saturable absorber was investigated in the early stages of the project whilst waiting for the components for the high-power diode-stack pump source to be delivered. This work was not originally intended to be part of the project, but is relevant since it demonstrate the potential for fiber lasers as Q-switched sources.

The fiber laser configuration used in our experiments (shown in figure 13) employed ~2m of Er,Yb doped double-clad fiber (EYDF) and an external cavity comprising a collimating lens (L_2) of 4.5mm focal length, a focusing lens (L_3) of focal length 8.6mm to focus the fiber output into the Co^{2+}:ZnS crystal, a second collimating lens (L_4) of focal length 15mm to re-collimate the beam, and finally, a diffraction grating, blazed at 1.55μm with 600 lines/mm, used in Littrow configuration to provide wavelength selective feedback. The focal lengths of lenses L_2 and L_3 were chosen to roughly minimize the mode volume in the Co^{2+}:ZnS crystal in order to obtain a low threshold for passive Q-switching. The EYDCF had a phospho-silicate core of 11μm diameter and 0.21 NA, and was surrounded by a pure silica inner-cladding of diameter 125μm. The outer-cladding was fabricated from a low refractive index (n=1.375) UV curable polymer resulting in a high NA (~0.49) for the inner-cladding. The EYDF was pumped by a beam-shaped diode-bar at 915nm with 8W of maximum power. The pump light was coupled into the fiber through a perpendicularly cleaved end-facet via an arrangement comprising two dichroic mirrors, with high reflectivity (~100%) at 915nm and high transmission (>95%) at 1.5-1.6μm, and a gradient-index lens (L_1) of 25mm focal length with anti-reflection coatings at the pump and

lasing wavelengths. The diffraction grating and cleaved fiber end-facet provided the feedback required for laser oscillation, with the end-facet serving as the output coupler. The use of a large diameter (multimode) core is attractive since it allows greater energy storage than conventional single-mode core designs [8], but obviously has the disadvantage that the beam quality is degraded due to multimode lasing. To suppress lasing on higher-order modes, a short length (~400mm) of standard single-mode fiber with a core diameter of 8μm was spliced on to the EYDF end adjacent to the external cavity. The end-facet of the single-mode fiber was angle-cleaved at ~15º to suppress parasitic lasing between the fiber end-facets. By bending the EYDF in a figure-of-eight in order to improve the overlapping of the pump modes with the fiber core, the absorption efficiency of the launched pump power was 95%.

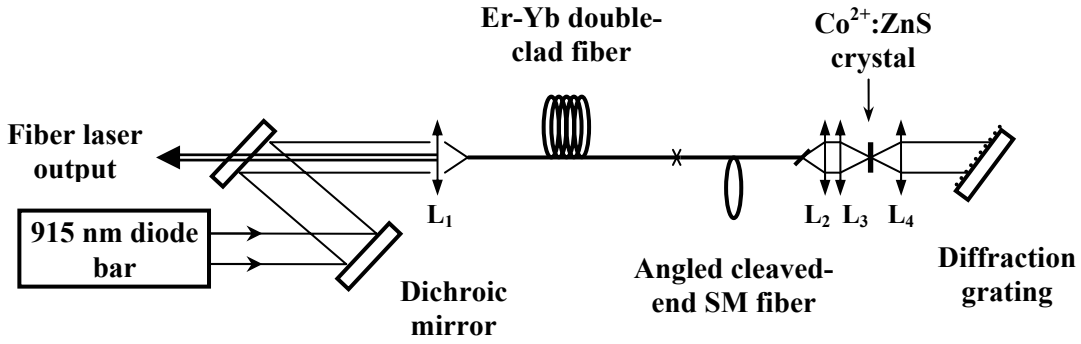

Figure 13: Passively Q-switched Er,Yb fiber laser

Co^{2+}:ZnS was chosen as the saturable absorber because it has a long metastable lifetime (≈200μs) and a high ground state absorption (GSA) cross-section (~9×10^{-19}cm^2), and hence it has a very low saturation fluence (0.145J/cm^2 at 1.53μm) [9]. In addition, it has very low non-saturable losses (<0.1cm^{-1}) compared to other saturable absorber Q-switches, and its absorption spectrum covers a broad wavelength range (1200nm – 1900nm), making it a suitable candidate for tunable Er^{3+} lasers systems operating in the 1.5-1.6μm spectral region. The Co^{2+}:ZnS crystal used in our experiments was 1mm thick and had uncoated facets. The small signal transmission at 1.534μm was only 9.5% and hence CW lasing is suppressed even with the high gain obtained with the EYDF amplifying medium.

Under the above operating conditions, we found that the threshold for passive Q-switching was ~600mW of absorbed pump power. The average output power and pulse repetition rate as function of absorbed pump power is shown in figure 14. The average slope efficiency was ~13% with respect to the absorbed pump power. One interesting feature of the laser was that the Q-switched pulse duration (~3.5-5ns) was much shorter than the cavity round-trip time (~25ns) and did not vary significantly with pump power. A typical Q-switched pulse (see inset of figure 15) comprises a main pulse with much lower power satellite pulses before and after the main pulse. At the maximum pump power, the pulse energy was found to be ~60μJ, with 75% contained

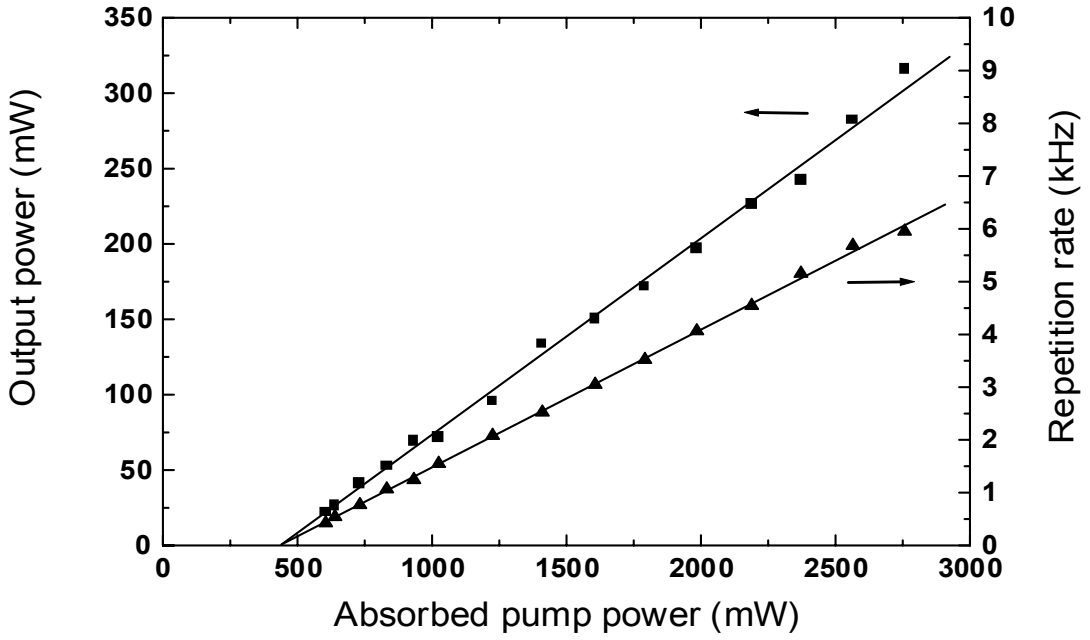

Figure 14: Average output power (square) and pulse repetition rate (triangle) versus the absorbed pump power

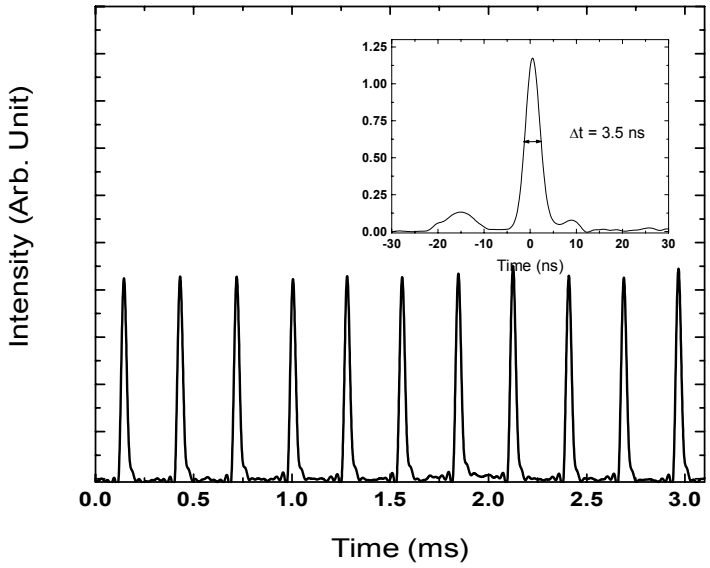

Figure 15: Typical Q-switch pulse train and its corresponding temporal pulse shape (inset).

within the main pulse, and corresponds to a peak power of more than 10kW. This is by far the highest peak power ever reported to date for any Q-switched Er^{3+} fiber laser. In addition, the operating wavelength could be tuned from 1532nm and 1563nm by simply adjusting the angle of the diffraction grating.

For comparison, the CW laser performance was also evaluated with the Co^{2+}:ZnS crystal removed from the external cavity while keeping all the other optical components in place. Under these operating conditions the CW slope efficiency was measured to be 15 %, and hence only 2% higher than for the passively-Q-switched laser. The low value for the CW slope efficiency can be easily explained by the extra resonator losses in the external cavity due to the grating, the collimating and focusing lenses and also, the single-mode fiber. It is worth noting that when the same fiber was employed in a simpler cavity configuration, where feedback for laser oscillation was provided by a high reflectivity mirror butted to one end of the fiber and by a perpendicularly-cleaved fiber end facet, we obtained a slope efficiency with respect to absorbed pump power of 46 %. Thus, by improving the design of the external cavity and using lower loss components, and modifying the design of the EYDF, it should be possible to construct a passively Q-switched EYDF laser with much higher efficiency. Further details of this work can be found in Appendix A1.

3.5 Tunable Er,Yb fiber laser

The main goal of this part of the project was to develop a high-power EYDCFL suitable for in-band pumping of an Er:YAG laser. In addition to the requirement for high-power (>10W) and high efficiency, the operating EYDFL operating wavelength had to be tunable to 1532nm to coincide with the absorption peak in Er:YAG to allow efficient pump absorption. This wavelength is at the short wavelength end of the emission spectrum in Er,Yb phospho-silicate fibers and hence meeting all of these requirements simultaneously is quite challenging. To identify the best route to the required lasing characteristics we fabricated a number of different fiber preforms with different Er and Yb ion concentrations selected according to the design strategy developed in section3.3 and evaluated these fibers in cladding-pumped laser configurations pumped by our 940nm diode-stack modules. All of the fibers had am Er,Yb-doped phospho-silicate core with NA of ~0.22 and diameters in the range 21-30μm, surrounded pure silica D-shaped inner-cladding with an outer diameter of ~350-400μm. The latter was surrounded by a low refractive index polymer outer-cladding resulting in a calculated NA of ~0.49 for the inner-cladding pump guide.

The first perform fabricated (LF42) had an Yb ion concentration of $\sim 1.31\times10^{20}cm^{-3}$ (estimated from a measurement of the effective pump absorption coefficient at 915nm) and a ratio of Yb ion to Er ion concentration of ~20 (estimated from the initial solution concentrations) to be ~20. However, when this fiber was tested in a simple (non-tunable) cavity configuration pumped by a 940nm pump module, it was found to lase at ~1μm and ~1.5μm with slope efficiencies with respect to absorbed pump power of 45% and 30% respectively. This indicated that energy transfer from Yb^{3+} to Er^{3+} ions was not very efficient in this fiber.

In an attempt to suppress lasing at 1μm, a second preform (LF59) was fabricated with a higher Yb concentration ($\sim 2.2\times10^{20}cm^{-3}$) and a with a lower Yb/Er concentration ratio (~5) to improve the energy transfer efficiency. The resulting fiber had a 24μm diameter core doped with a numerical aperture of 0.21 and a ~400μm diameter pure silica inner-cladding with an outer dimension ~400μm and with a D-shaped cross-section to promote efficient pump absorption. The fiber was tested in a simple tunable cavity configuration (shown in figure 16) consisting of

an 18m length of EYDCF and an external cavity. The latter comprised an anti-reflection coated collimating lens of focal length, 25mm, and replica diffraction grating with 600 lines/mm mounted on a copper substrate to facilitate removal of waste heat. The grating was blazed for a

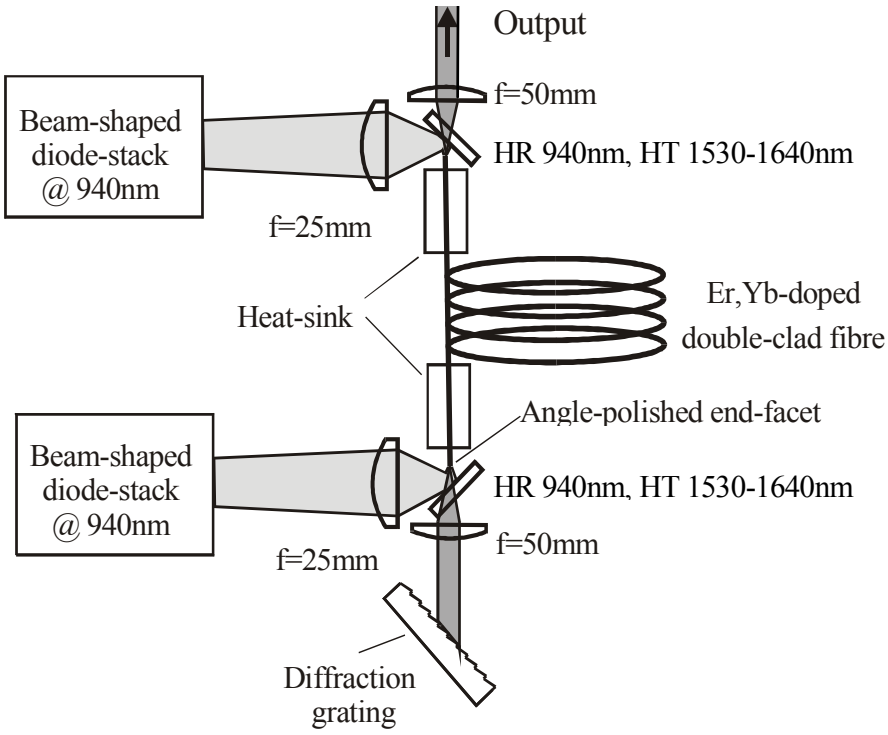

Figure 16: Tunable Er,Yb fiber laser configuration

wavelength of ~1.65μm with reflectivity ~75% for light polarised parallel to the grooves and ~95% for light polarised in the orthogonal direction, and was aligned in the Littrow configuration to provide wavelength selective feedback and hence the means for adjusting the lasing wavelength. The fiber end facet nearest the external cavity was angle-polished at ~12.5º to the fiber axis to suppress parasitic lasing between the two fiber ends. Light emerges from this end of the fiber at an angle ~18º to the fiber axis, so it is also extremely important to carefully align the collimating lens in the external cavity at the same angle and in the appropriate position in order to avoid lens aberrations, which would otherwise reduce the feedback efficiency and hence limit the tuning range. The opposite end of the fiber was polished perpendicular to the fiber axis to provide the feedback necessary for lasing. The latter acted as the output coupler with its high transmission (~96.5%) dominating over the external cavity losses. The EYDF was pumped through both fiber end facets by the diode-stack pump modules described in section 3.2. After the beam conditioning optics, each diode-stack module provided a pump power of ~65W, of which ~50W was coupled into each end of the EYDCF with the aid of a 25mm focal length high numerical aperture (GRADIUM) lens and a dichroic mirror to separate the signal light from the

pump light. This arrangement, with separate pump focussing and external cavity lenses, has the attraction that it allows independent optimisation of pump launching efficiency and alignment of the external cavity. The effective absorption coefficient for the fiber at 940nm was determined via a cut-back measurement to be ~0.43dB/m and hence a rather long length of fiber ~18m was required for efficient pump absorption (~83%), and to prevent unabsorbed pump from one pump source entering, and possibly damaging, the other pump source. A photograph of the experimental set-up is shown in figure 17.

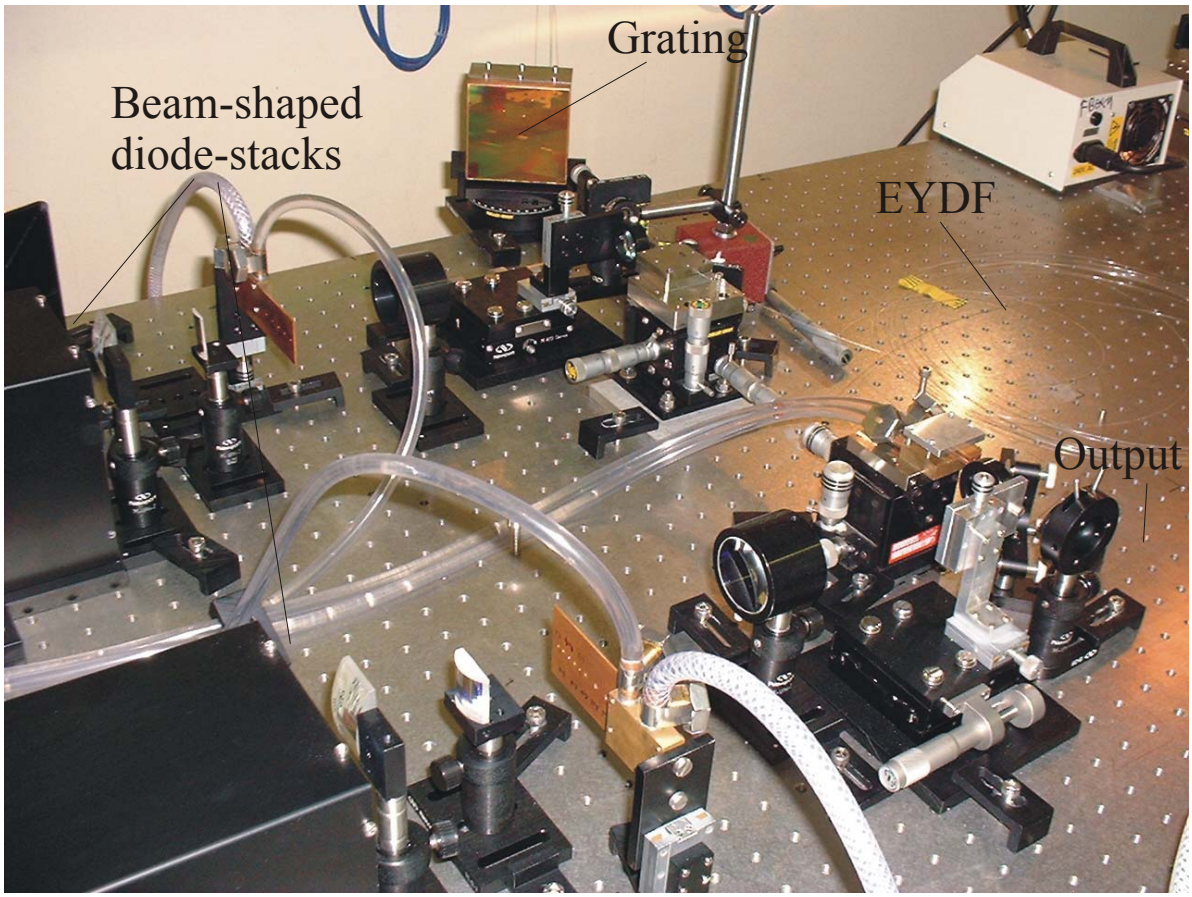

Figure 17: Tunable Er,Yb-doped silica fiber laser set-up

Under these operating conditions, the EYDFL had a threshold pump power of ~3W (absorbed) and at the maximum available pump power (corresponding to 83W absorbed) yielded 30W of output at 1570nm (see figure 18). The slope efficiency with respect to absorbed pump power was ~39%, which compares favourably with best efficiencies obtained in our low power Er,Yb-doped fiber laser experiments described in section 3.3. Furthermore, there was no evidence of lasing on the Yb^{3+} transition at ~1µm, implying efficient energy-transfer from Yb^{3+} to Er^{3+}. It should be noted that in an earlier experiment using an EYDCF pulled from the same perform in a non-tunable cavity configuration that lasing a ~1µm was observed albeit with a very low slope

efficiency (~5%) compared to ~1.5μm laser emission. This is a significant improvement over the previous fiber pulled from perform LF42. However, wavelength discrimination (as provided by our external cavity in this case) is required for complete suppression of ~1μm lasing on the Yb^{3+} transition. Using the tunable cavity configuration (shown in figure 16), the EYDFL operating wavelength was tuned, by adjusting the angle of the diffraction grating, over 66nm from 1562nm to 1627nm (figure 19). It should be noted that the operating wavelength range is

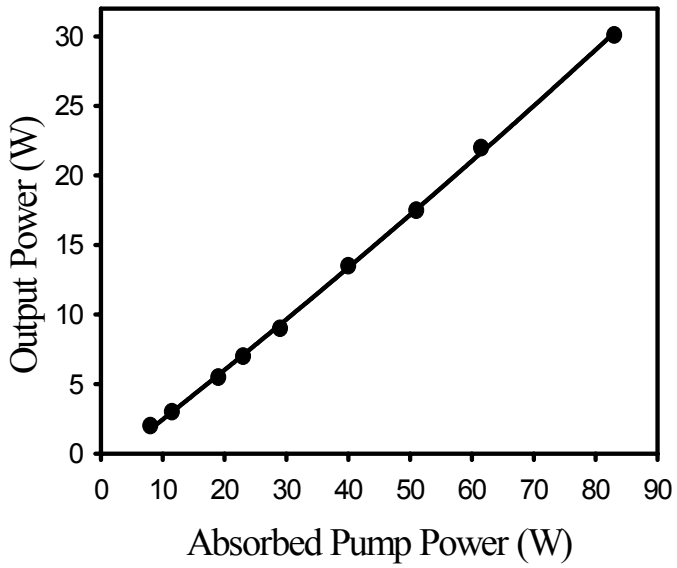

Figure 18: EYDCFL output power at 1570nm versus absorbed pump power

displaced towards the long-wavelength side of the emission line, which peaks at ~1535nm. This is due a combination of increased reabsorption loss at shorter wavelengths and gain saturation due to amplified spontaneous emission at longer wavelengths, which result from the need to use a relatively long fiber for efficient pump absorption. One interesting feature of the tuning curve (figure 19) is that there is a pronounced decrease in output power towards longer wavelengths (i.e. from 30W to 19W as the wavelength is tuned from 1568 to 1620nm). The origin of this behaviour is unclear, but could be explained by increased loss at longer wavelengths. The laser spectrum (see inset of figure 19) was typically composed of a number of relatively sharp lines of width, 0.03nm (FWHM), spread over a total width of 0.6nm. The output beam had beam quality factor, M^2, of 2.9 due to the slightly multimode nature of the core, which had a V parameter of 10. However, another contributing factor to the poor beam quality was thought to be spherical aberration of the collimating lens in the external cavity causing some of the light to be fed back into the inner-cladding. By placing an aperture in the external cavity, between the collimating lens and grating, to reduce the beam size we achieved a further decrease in the M^2 value to 1.8 for only a small reduction (~10%) in the output power. It should be noted that the beam quality factor for the EYDCFL output could be even lower, since it is likely that it is degraded by the collimating lens. These results show that with careful optimisation of the EYDCFL design it is possible to achieve relatively good output beam quality, even with a highly multimode core.

Further details of this experiment will appear in a paper which has been accepted for publication in Electronics Letters (see Appendix A2).

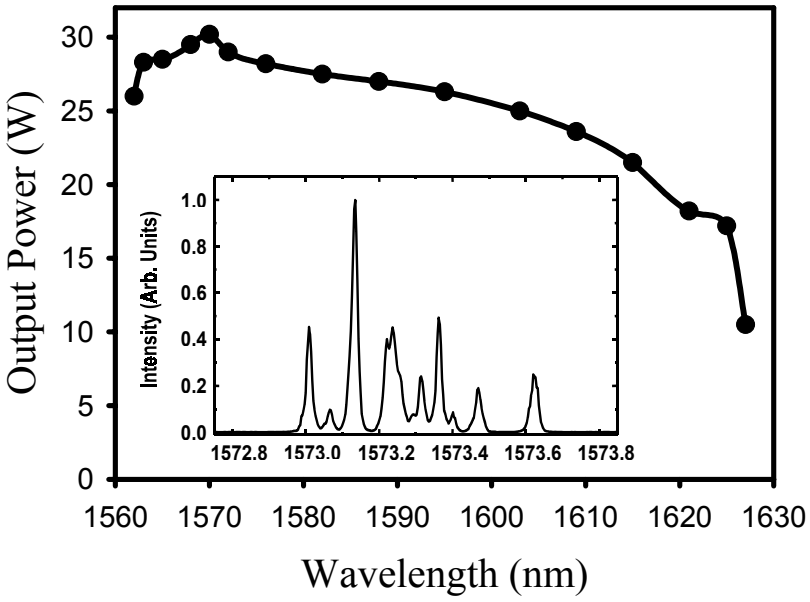

Figure 19: EYDCFL output power versus wavelength

However, it was not possible to tune to wavelengths shorter than 1568nm with this fiber. Extension of the tuning range to shorter wavelengths should be possible by employing diode-stacks with pump wavelength at the absorption peak (~975nm) where the absorption coefficient is approximately six times larger (see figure 20), which allows a much shorter fiber with reduced

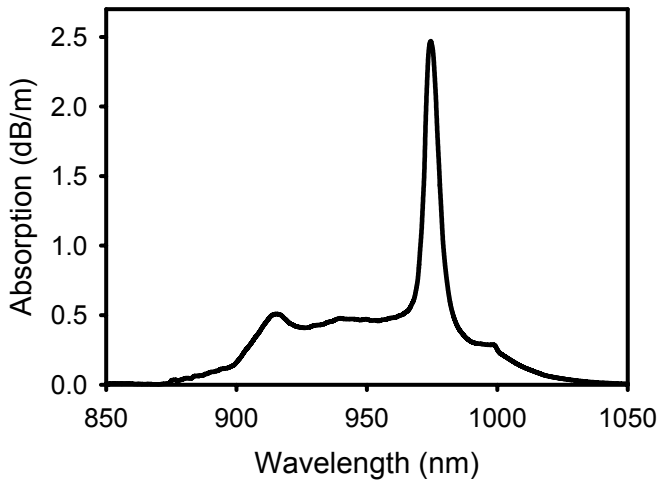

Figure 20: Absorption coefficient versus wavelength in Er,Yb-doped phospho-silicate glass

re-absorption loss at shorter wavelengths and reduced gain at longer wavelengths. Unfortunately, at the time this project commenced diode-stacks at 975nm were not commercially available. We have therefore had to adopt a different strategy, which involves using an EYDCF with reduced Er^{3+}-doping level and increased Yb^{3+}-doping level. The rationale for this is that it should be possible to excite a larger fraction of the Er ions and hence reduce the re-absorption loss at shorter wavelengths, allowing shorter wavelength operation. This assumes that the energy transfer efficiency from Yb to Er ions is not decreased significantly. To investigate this approach we fabricated another preform (LF 69), with a higher Yb/Er concentration ratio ~10 and nearly a factor-of-three higher Yb ion concentration. The resulting EYDCF had a D-shaped inner-cladding diameter of ~400μm and a core diameter of ~30μm, and the effective absorption coefficient for pump light at 940nm was determined via a cut-back measurement to be ~1.2dB/m.

The fiber was tested in the same tunable cavity arrangement as employed for the previous fiber (see figure 16). However, due to the higher Yb concentration, a much shorter length of fiber (~8m) was required to absorb ~90% of the launched pump light at 940nm. Pump light from the two diode-stacks at 940nm was coupled into both ends of the Er,Yb fiber as for the previous EYDCFL. In order to prevent the polymer outer coating of the fiber burning due to stray (un-coupled) pump light, 1-2cm of the coating was removed from both ends of the fiber and the uncoated sections were left protruding from water-cooled heat-sinks, which cooled the next 4-5cm of fiber. A similar arrangement was employed in the previous laser and has generally worked quite well in the past. However, on this occasion we experienced some problems with the fiber damaging due to the coating burning at the heat-sink. We concluded that this was probably due a slight change in the pump in-coupling arrangement, allowing high NA modes to be launched into the protruding sections of fiber, which were then absorbed in the coating since they could no longer be guided. This problem was solved by simply using longer focal length pump focusing lenses to reduce the pump beam divergence, without degrading the launch efficiency and laser performance.

Figure 21 shows the output power versus wavelength at diode drive currents of 30A and 40A, corresponding to absorbed pump powers of ~45W and ~68W respectively. With a drive current of 30A, the tunable Er,Yb fiber laser yielded a maximum output power of 13.5W at ~1568nm, but with little variation in power over the wavelength range 1545-1572nm. With a drive current of 40A, we obtained up to 23W of output and a very similar tuning range. Beyond this wavelength range the fiber laser power drops very rapidly. We decided not to measure fiber laser output power versus wavelength at the maximum drive current of 50A, since on a number of earlier occasions we experienced damage to the fiber end facets (probably due to production of a high energy pulse) when the laser is operated at the end of tuning range (i.e. where the output power drops and hence greater energy is stored in the fiber). Our strategy was, instead, to determine the tuning range at lower pump powers to establish the 'safe' tuning range over which damage could be avoided before operating at higher power levels. In this case, we concluded that the shortest operating wavelength for our fiber was ~ 1547nm. Figure 22 shows the output power at 1547nm versus pump power. The fiber yielded a maximum output power of ~32W for ~90W of absorbed pump power and the slope efficiency with respect to absorbed pump power was ~40%. The high slope efficiency in combination with the absence of any lasing on the Yb^{3+} transition at ~1μm indicates that the energy transfer efficiency from Yb^{3+} to Er^{3+} has not been

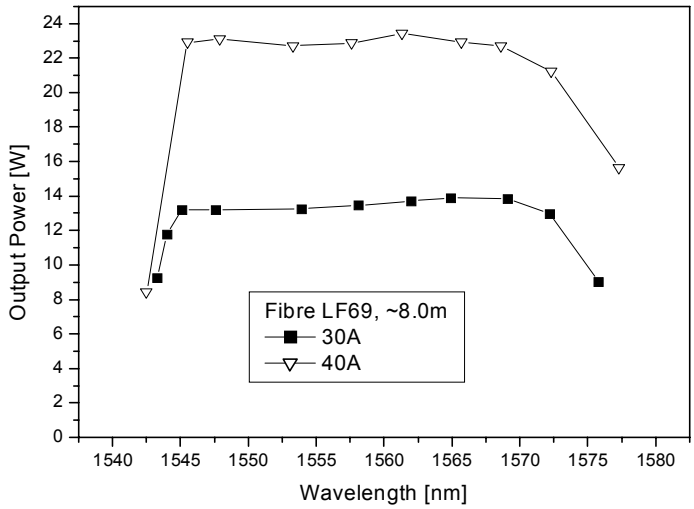

Figure 21: Output power versus wavelength for the tunable Er/Yb fiber laser

degraded by increasing the Yb and reducing the Er concentration. Unfortunately, whilst were successful in decreasing the shortest operating wavelength by ~20nm to 1547nm, it was not possible to reach the target wavelength of 1532nm without using a much shorter length of fiber at the expense of a significant reduction in the efficiency due to decreased pump absorption.

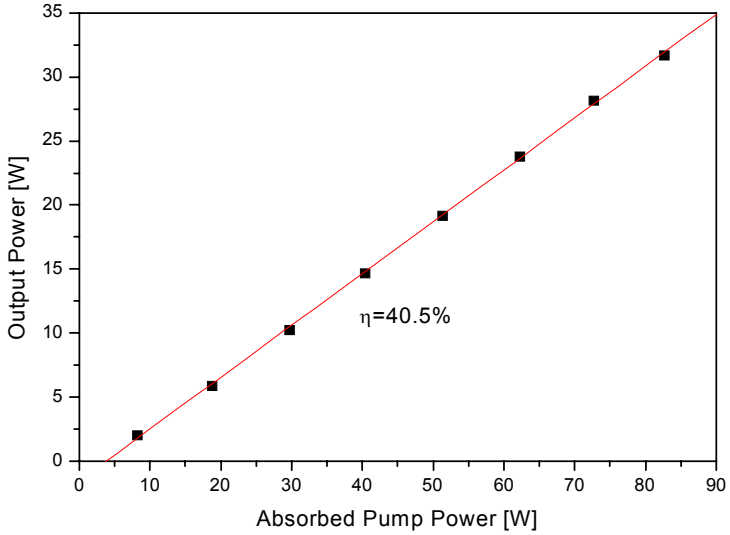

Figure 23: Output power versus pump power for the tunable Er/Yb fiber laser at 1547nm.

To further decrease the operating wavelength a fourth perform (LF125) was fabricated following the same design strategy outlined earlier (i.e. with increased Yb concentration and a much higher Yb/Er concentration ratio of ~17 compared to perform LF69). The resulting fiber had a core diameter of 30µm and a D-shaped inner-cladding of diameter, 400µm, as before. A simple cut-

back measurement indicated that the effective absorption coefficient for the pump at 935-940nm was increased to 1.7dB/m indicating that the Yb concentration was ~1.4 times greater than for the previous fiber. The fiber was tested in the tunable cavity arrangement (shown in figure 16), but with only one pump diode present. Figure 24 shows the tuning curves obtained for different lengths of fiber in the range 3.5-6m corresponding to pump absorption efficiencies in the range 75-90%. It can be seen that the target wavelength of 1532nm can be reached by selecting a fiber length of <4m. However, the efficiency is rather low compared to the efficiency at longer wavelength (~1565nm). Shortening the fiber length further will also increase the efficiency at

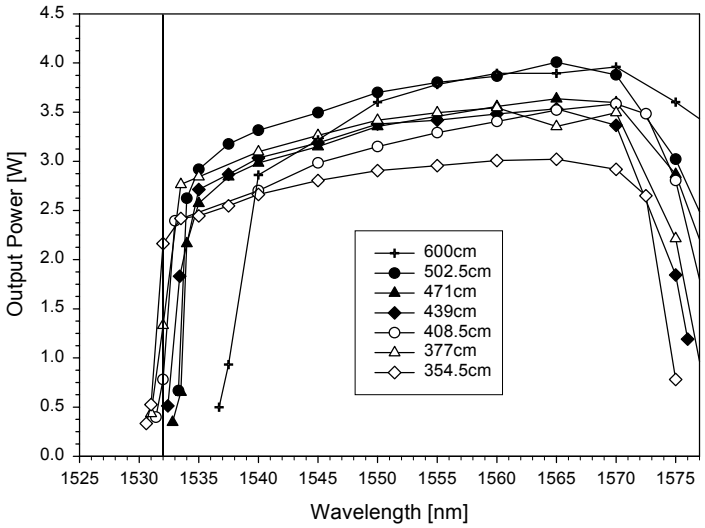

Figure 24: Tuning range for new fiber (LF125) as a function of fiber length.

1532nm with respect to absorbed pump power, but at the expense of a reduction in pump absorption efficiency, and hence a reduction in the overall efficiency. A similar experiment performed with the previous fiber from perform LF69 revealed that a shorter length of fiber (<2.5m) with reduced pump absorption efficiency (<50%) was required for operation at 1532nm. Thus, the fiber from perform LF125 is better suited to our requirements, but the pump absorption efficiency was not high enough to allow pumping with both pump modules from opposite ends.

In addition to the above experiments we have also conducted a detailed experimental study of the temporal stability of the tunable EYDCFL output. In typical operating conditions, the output power is relatively stable with amplitude fluctuations of less than 5% over a timescale of several minutes. However, at the edge of the tuning range the power stability is somewhat worse, and, in some instances, self-pulsing can occur resulting in damage to the fiber end facets. For this reason, extreme care needs to be taken when tuning the wavelength towards the limits of the tuning range at high pump powers.

We have also investigated the temporal stability of the output spectrum. One interesting observation was (discussed earlier) was that the wavelength spectrum consisted of a number of discrete wavelengths of ~0.1nm width spanning a wavelength range of ~1nm. We have now

found that with careful alignment of the external cavity it is possible to narrow the output spectrum to a total width of ~0.4-0.6nm, which is less than the width of the Er:YAG absorption line at 1532nm. To study the temporal stability of the output spectrum, the lasing wavelength was tuned to 1545nm and the feedback cavity was aligned to minimize the spectral width of the output. Output spectra recorded at one-minute intervals are shown in figure 25. It can be seen that the power distribution between the various lines changes considerably during the 18 minute time span recorded, but the total wavelength spread remains fixed at <1nm. We believe that this behaviour may be linked with temporal changes in the number of high-order modes oscillating, and hence the beam quality, due to movement of the fiber end nearest the external cavity. The latter may be a result of mechanical vibration, or heating of the fiber end. Further studies are needed to confirm this and, if appropriate, find a remedy for the problem. Temporal changes in the output spectrum should have little, if any influence on the Er:YAG laser performance. However, if the beam quality changes this could lead to a change in output power from the Er:YAG laser and hence could be a problem.

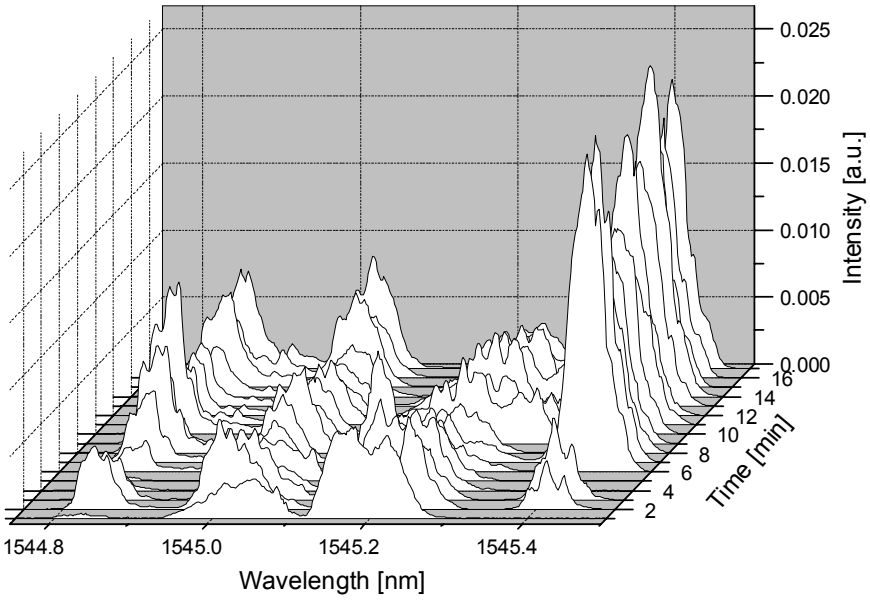

Figure 25: Temporal evolution of the output spectrum of a tunable EYDFL.

To maximize the EYDCFL power attainable at 1532nm for pumping an Er:YAG laser we adopted a slightly modified cavity design (shown in figure 26) with a relatively short length (~2.55m) of fiber from perform (LF125). For this length of the fiber the single-pass pump absorption efficiency was ~69%. To improve the overall pump absorption efficiency, the unabsorbed pump light after a single pass was separated from the signal light at 1532nm using a dichroic mirror and retro-reflected for a second pass of the fiber using a simple external cavity arrangement. Using this arrangement, we estimate that the pump absorption efficiency was increased to ~90%. To achieve stable and efficient operation at 1532nm it is extremely important to have efficient and strongly wavelength selective feedback from the grating,

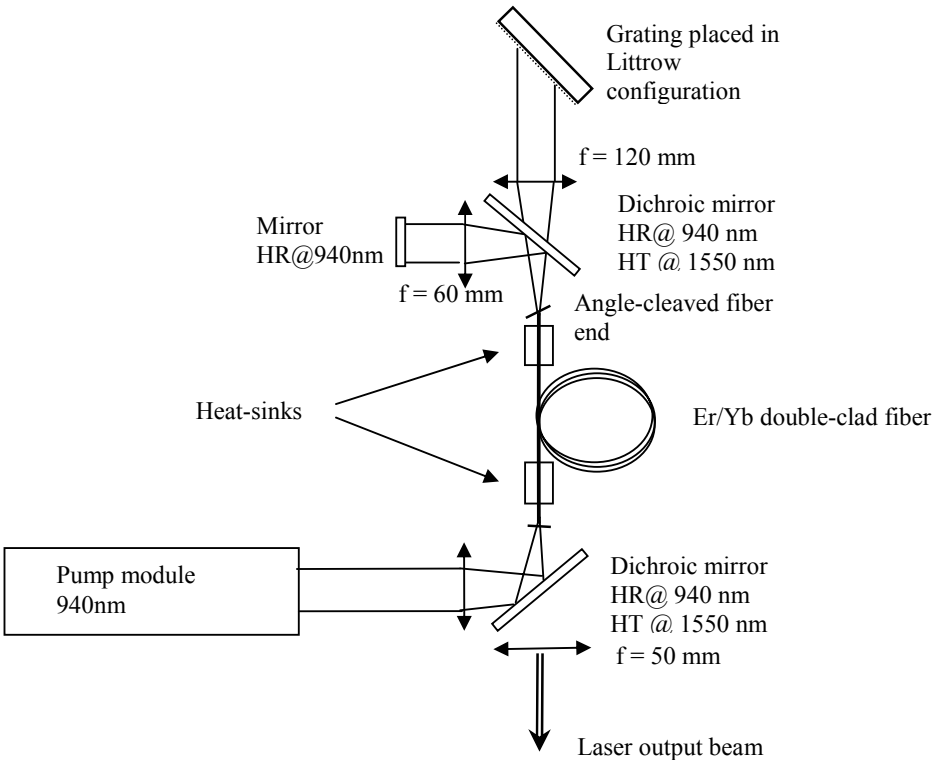

Figure 26: Tunable EYDCFL set-up

otherwise the inversion may be depleted by parasitic lasing at longer wavelengths or ASE. To improve the feedback efficiency and increase the spectral selectivity of the external cavity, the 50mm focal length collimating lens employed in the previous set-up was replaced by one with a longer focal length (~120mm) and larger diameter (~50mm). The longer focal length makes it possible to set up the feedback arm in 'relay imaging' configuration, where the distance from the lens to the grating is equal to the focal length. This configuration reduces the distortion of the image of the fiber core reflected back on to the fiber end facet and hence can improve the efficiency of the feedback loop. Moreover, the use of a longer focal length collimating lens results in a larger beam size on the grating and reduced beam divergence, and hence provides better wavelength discrimination. This new arrangement was found to be much easier to align than the previous set-up, and showed improved wavelength and intensity stability. The output power was stable to ±2% over a 20min trial period at ~9W output power. In addition, the wavelength was stable at 1532.5nm with less than 0.1nm shift over several weeks while the Er:YAG laser experiments were conducted. The main disadvantage of this cavity configuration was that the pump power was limited to ~54W (launched). Nevertheless, the EYDCFL yielded a maximum output power of 18W at 1532nm and the slope efficiency with respect to launched pump power was ~36% (see figure 27). A much higher slope efficiency (~46%) with respect to absorbed pump power was achieved with single-pass pumping configuration indicating that the arrangement for retro-reflecting the unabsorbed pump light after a single-pass in figure 26 is not

optimum. Thus, with an improved design there is scope for a significant improvement in the overall efficiency.

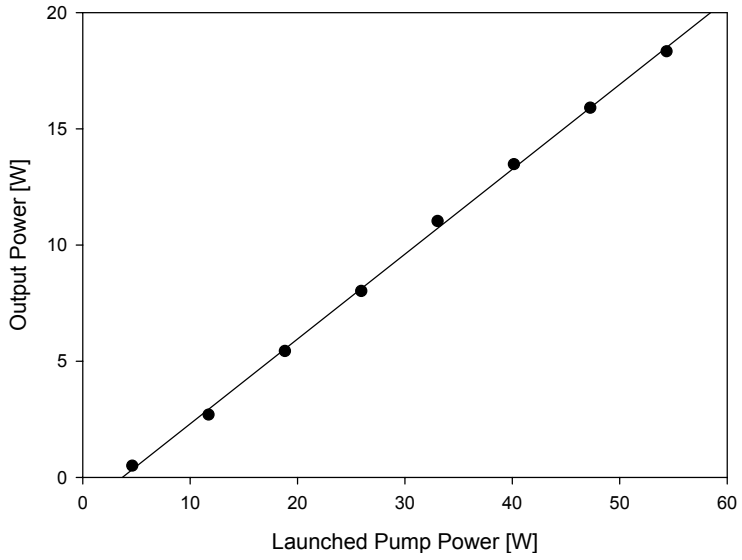

Figure 27: Output power versus launched pump power for the EYDFL at 1532nm

3.6 Prospects for further power scaling

At present the maximum power at attainable from our tunable EYDCFL at 1532nm was limited by the pump power that could be absorbed in the required length of fiber. There are a number of ways to increase this power level as follows:

(a) A high-power diode source with better beam quality would allow efficient launching into a fiber with a smaller inner-cladding and hence a smaller cladding-to-core area ratio. This would increase the effective pump absorption coefficient and hence decrease the fiber length required for efficient pump absorption. The beam quality factors for our present diode-stack pump modules are limited mainly by the positioning accuracy of the fast-axis collimating lenses. There scope for improving the beam quality factor in the fast-direction (and hence the brightness) by at least a factor-of-four by employing a better jig for aligning and fixing the microlenses in position. In addition, there is also scope for improving the beam quality factor in the orthogonal direction by at least a factor-of-three by using low fill-factor diode-stacks following by slow-axis lens arrays for collimating the beams from each emitter in the slow direction, and by a further factor-of-two by using polarization multiplexing.

(b) Using a diode source at 975nm to coincide with the absorption peak in Er,Yb-doped phosphor-silicate glass would decrease the length of fiber required for efficient pump absorption. Diode-bars and diode-stacks with operating wavelengths in the 975-980nm are now commercially available from a number of vendors. Even allowing for the relatively narrow

bandwidth of this absorption peak (~9nm) and the linewidth of the diode pump emission it would be reasonable to expect an increase in the effective absorption coefficient by more than factor-of-four compared to a 940nm pump source.

(c) Further optimization of the Yb and Er ion concentrations following the strategy outlined in the previous section (i.e. by increasing the Yb concentration and decreasing the Er concentration). This would serve to further increase the Er excitation density (assuming that the Yb to Er energy transfer efficiency is not degraded) and would reduce length of fiber required for efficient pump absorption, serving to reduce the gain at longer wavelengths and increasing the gain at shorter wavelengths. This approach has so far proven to be very successful without any evidence of a reduction in efficiency due to a reduction in the energy-transfer efficiency. Clearly, there will be a limit to how far one can increase the Yb concentration and decrease the Er concentration before there will be a detrimental impact on the energy-transfer efficiency. This is difficult to predict, but our experimental results so far suggest that there is still scope for further optimization of the core composition.

Adopting the strategies outlined above should allow scaling to output power levels at 1532nm well in excess of a hundred watt, with the upper-limit on power determined by the onset of thermally-induced damage and/or self Q-switching.

4.0 Fiber laser pumped Er:YAG laser

4.1 Introduction

There are many applications which would benefit from the availability of an efficient laser source capable of generating high pulse energies in the ~1.5-1.6μm eyesafe spectral regime for relatively modest pump powers. Er:YAG is an attractive candidate as the laser medium owing its robust thermo-mechanical properties and long fluorescence lifetime (~6.5ms) [10] for the upper laser manifold ($^4I_{13/2}$) for the 1646nm laser transition. A further attractive feature is that it is possible to pump directly into the upper manifold owing to a strong absorption peak at 1532nm which is conveniently accessible by high-power Er-doped fiber sources (see figure 28). This suggests that the heat loading in Er:YAG should be very low owing to the small quantum defect (~7%) opening up the prospect of very high lasing efficiencies. Recently, researchers from BAE Systems have demonstrated cw and Q-switched Er:YAG [11] and Er:LuAG [12] lasers, pumped (in-band) by an erbium fiber laser, with multi-watt average powers and slope efficiencies with respect to incident pump power up to 54% and 40% respectively. It is worth noting that a similar fiber-bulk hybrid laser approach applied to a Ho:YAG lasers pumped by a Tm fiber laser has resulted in even higher slope efficiency (~80%) [13] in spite of a higher quantum defect (~9%). This raises the obvious question as to whether similar or higher efficiencies can be achieved in an in-band pumped Er :YAG laser. The main aim of our work was to study how various factors (and in particular Er doping concentration) affect laser performance with a view to establishing a design strategy for optimizing laser performance.

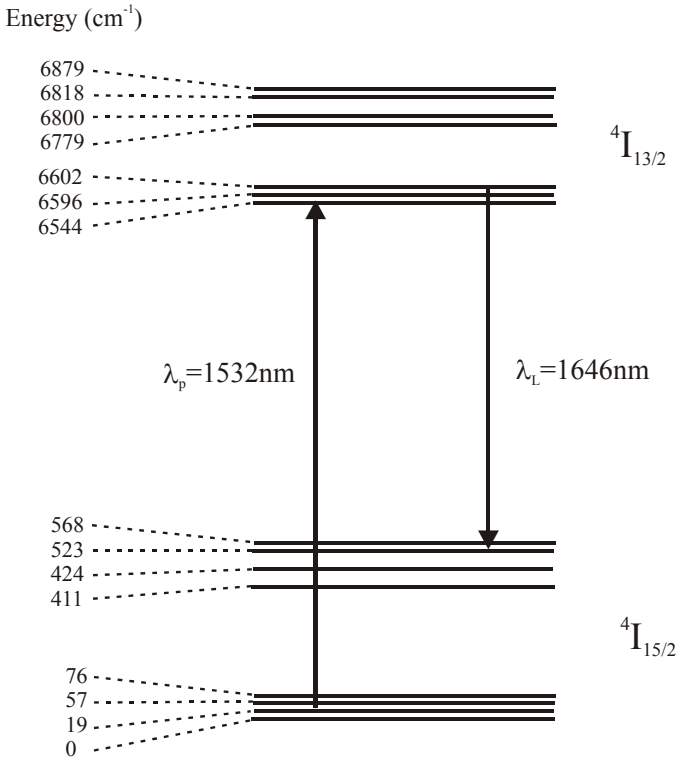

Figure 28: Energy level diagram for Er:YAG at 300K (taken from ref. 14)

4.2 Er:YAG laser design

The experimental arrangement used in our study is shown in figure 29. A relatively simple three-mirror folded-cavity design was used for the Er:YAG laser comprising a plane pump in-coupling mirror with high transmission (>95%) at the pump wavelength and high reflectivity (>99.8%) at the lasing wavelength (1646nm), a concave folding mirror with radius of curvature, 100mm, and high reflectivity in the 1560-1680nm regime and a plane output coupler with transmission 2%, 10%, 20% or 30% from 1560-1680nm. The Er:YAG crystal was mounted in a water-cooled copper heat-sink with cooling water maintained at a temperature of ~15ºC and was positioned ~0.5mm from the input coupler mirror. The optical path lengths from the input coupler to the concave mirror and from the concave mirror to the output coupler were selected to be 57mm and 165mm respectively. This arrangement resulted in a TEM_{oo} mode radius in the Er:YAG rod of 75μm, which was relatively insensitive to the thermal lensing. Pump light from the EYDCFL (shown in figure 26) was collimated by a 50mm focal length plano-convex lens and focused into the Er:YAG crystal using a 250mm plano-convex lens. The effective pump beam waist radius in the crystal was determined to be approximately 114μm. The M^2 parameter for the pump beam (after the collimating and focused lenses) was determined to be 2.5 and hence

the Rayleigh range ($z_{op}=\pi n w_p^2/M^2\lambda$) for the pump beam in the Er:YAG was ~19mm. In preliminary experiments no attempt was made to isolate the EYDCFL from back reflections from the Er:YAG laser. However, we found that the Er:YAG cavity acts as an external feedback cavity for the EYDCFL at wavelengths outside the Er:YAG absorption band and hence competes with the wavelength selection provided by the diffraction grating. The net result of this feedback

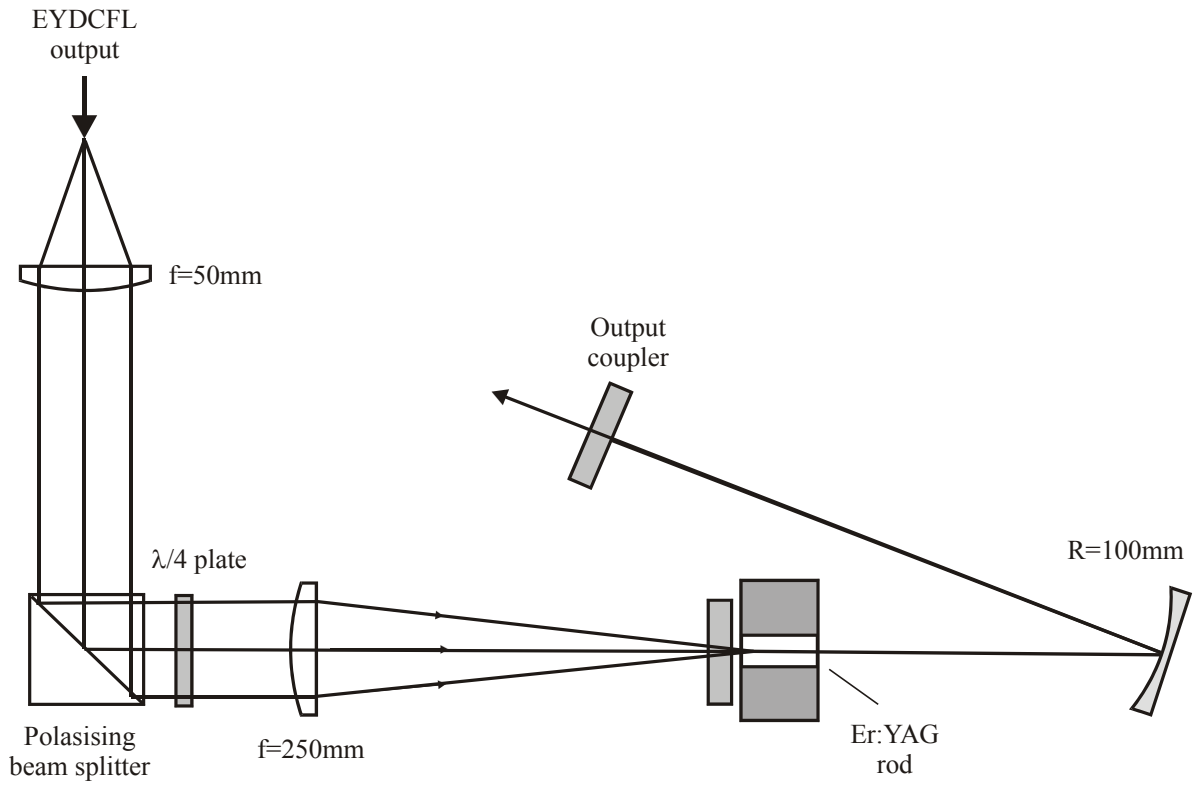

Figure 29: Er:YAG laser design

was that the EYDCFL operated at longer wavelengths to avoid the strong absorption peak in Er:YAG at 1532nm hence reducing the absorption efficiency. In spite of several attempts to improve the spectral selectivity of the grating feedback cavity to dominate over this wavelength selection mechanism we were unable able to maintain robust operation of the EYDCFL at 1532nm. To overcome this problem a simple isolator comprising a polarizer and quarter-wave plate was placed in the pump beam path between the collimating and focusing lenses for most of our experiments. This had the undesirable effect of reducing the available pump power from ~14W to ~6.5W since the EYDCFL output was not polarised. However, this proved to be sufficient for most of our preliminary experiments.

The performance of the Er:YAG laser was evaluated for a range of different Er^{3+} doping concentrations and different output coupling losses. In each case care was taken attenuate any unabsorbed pump light at 1532nm by reflecting the laser output from a plane mirror with the same coating specification as the pump in-coupling mirror. The Er:YAG output power was measured with a Molectron EPM1000 powermeter, and the incident pump power was monitored by measuring the power reflected from an inclined glass plate located between the pump collimating and focusing lenses with the aid of a Gentec powermeter. The readings for both output power and pump power were averaged over concurrent time spans of 50s to reduce the impact of any changes in the fiber laser output power and mode profile. The threshold pump power was measured directly as the pump power required for the onset of relaxation oscillations.

The Er:YAG laser rods used in our experiments were purchased from Scientific Materials Inc. and had doping concentrations of 0.5at.%, 1at.%, 2at.% and 4at.%. and respective lengths of 29mm, 15mm, 7.3mm and 3.8mm which were selected to be approximately equal to three absorption lengths for the pump light at 1532nm. All of the laser rods had a diameter of 2mm and had antireflection coatings for the wavelength range, 1.5-1.7μm, on both end faces.

4.3 Er:YAG laser performance

Figures 30 (a), (b) and (c) show the Er:YAG laser output power as a function of pump power for crystals with 0.5at.%, 1.0at.% and 2.0at.% Er^{3+} concentrations respectively. No laser emission was observed for the 4.0at.% crystal. The best performance was obtained using the 0.5at.% Er-doped crystal, which produced a maximum output power of ~1.6W at 1646nm for ~5W of

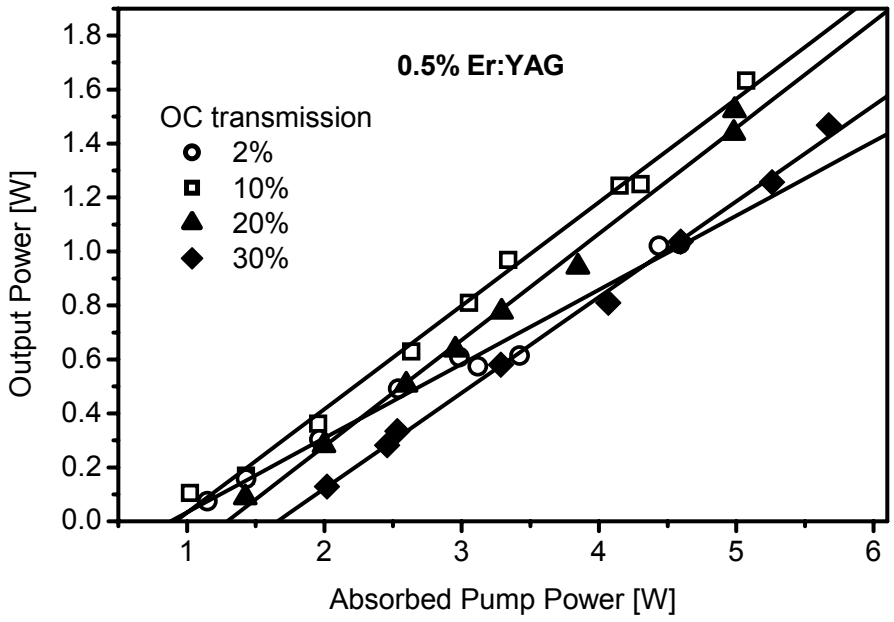

Figure 30(a): Output power versus pump power for 0.5at.% Er:YAG rod

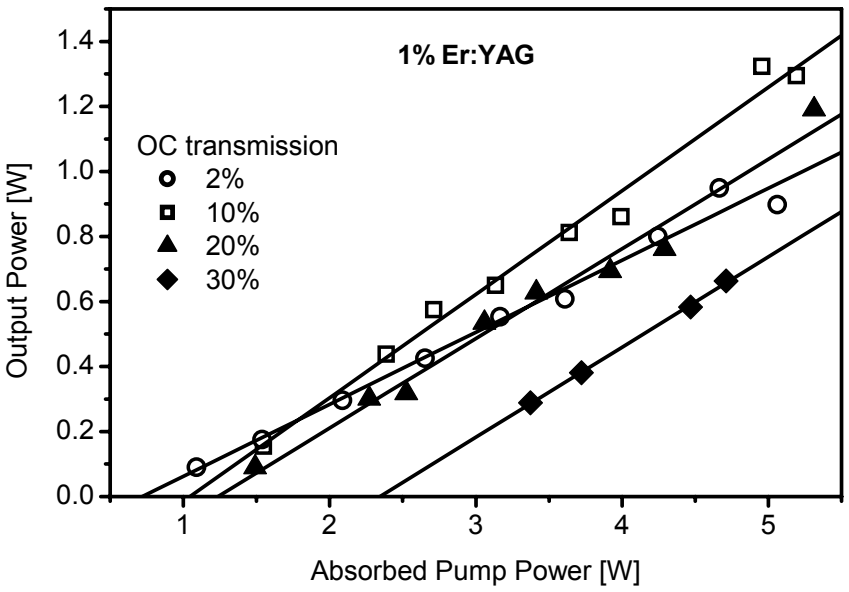

Figure 30(b): Output power versus pump power for 1.0at.% Er:YAG rod

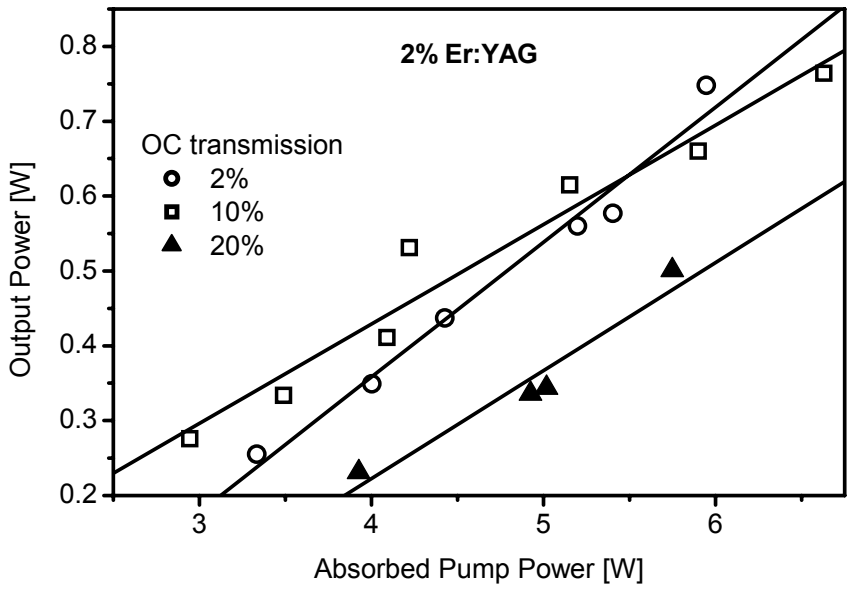

Figure 30(c): Output power versus pump power for 1.0at.% Er:YAG rod

absorbed pump power at 1532nm. This was obtained using an output coupler with a transmission of 10%. At the same pump power and with the same output coupler, lasers employing the 1.0at.% and 2.0at.% crystals produced only 1.3W and 0.56W of output respectively. These results indicate that there is a dramatic reduction in the overall efficiency with increasing Er concentration. The situation is better illustrated in figure 31 and 32 which show the dependence of threshold pump power and slope efficiency on Er concentration for different output coupler transmissions. It can be seen from figure 31 that there is a dramatic increase in the threshold pump power with increasing Er concentration and that the relative

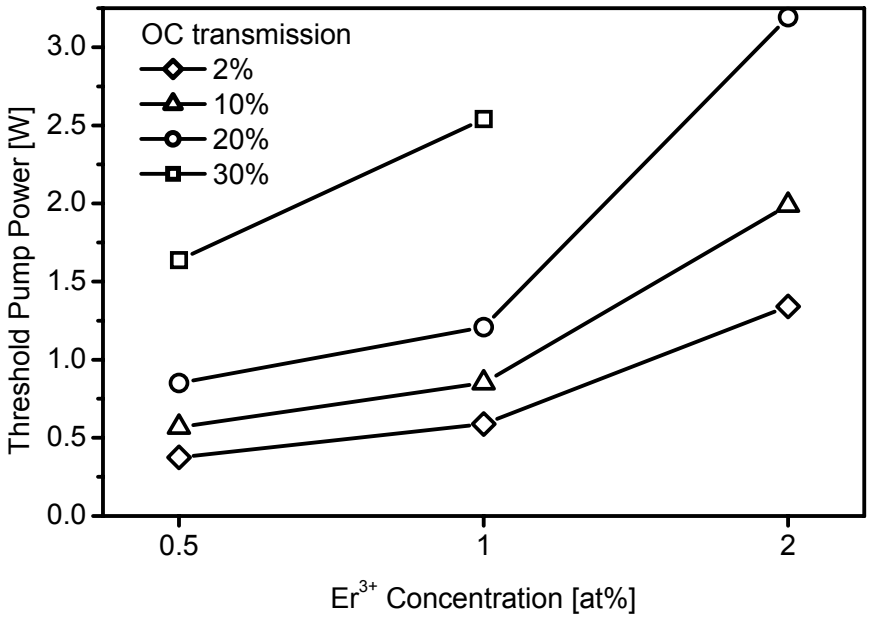

Figure 31: Er:YAG threshold pump power versus Er concentration

increase in threshold power increases with output coupler transmission (i.e. cavity loss). The 1646nm ($^4I_{13/2} \rightarrow {}^4I_{15/2}$) transition in Er:YAG is a quasi-three-level transition since the lower laser level resides in the ground state manifold. An approximate value for the threshold pump power, P_{pth}, can be calculated from [15]:

$$P_{pth} \approx \frac{\pi h\nu_p \left(w_p^2 + w_L^2\right)\left(L + T + 2f_1\sigma N_1 L_c\right)}{4f_2\sigma\tau_f\eta_{abs}} \tag{4}$$

where L_c is the length of the laser rod, w_p is the pump beam radius in the laser rod, w_L is the TEM_{oo} mode radius in the laser rod, L is the cavity loss, T is the transmission of the output coupler, N_1 is the population of the lower manifold, τ_f is the lifetime of the upper laser level, η_{abs} is the fraction of the incident pump power absorbed and f_1 and f_2 are the fractions of the populations of the lower and upper level manifolds which reside in the lower and upper laser

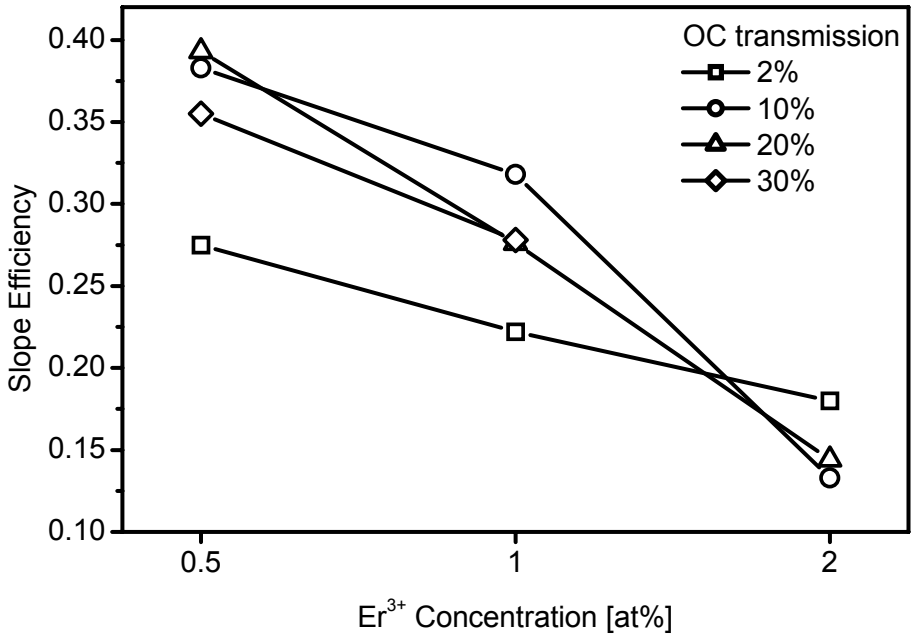

Figure 32: Er:YAG slope efficiency versus Er concentration

level respectively. This expression assumes that there is negligible ground-state depletion and that the total cavity loss is very small (i.e. L+T<<1). At room temperature, $f_1 \approx 0.02$ and $f_2 \approx 0.21$ for the 1646nm transition in Er:YAG. This suggests that approximately 8.7% of the Er ions must be excited to reach transparency. Taking $\sigma = 2\times10^{-20}cm^2$ and assuming that the round-trip cavity loss (excluding the output coupling loss) is ~1%, we estimate from equation (4) that the threshold pump power for our Er:YAG laser with an output coupler transmission is ~0.2W and is independent of the Er concentration. The latter results from the fact that N_1L_c is approximately the same for all of the rods investigated. It is worth noting that just over half this threshold power is required to reach transparency. The calculated threshold is much lower than we achieve in practice even for the lowest Er concentration. The fact that the threshold pump power increases so dramatically with Er concentration is a very surprising result. There are a number of factors which could contribute to this effect as follows:

(a) The passive loss for the Er:YAG rods could be much larger than expected and concentration dependent. However, we have roughly measured the cavity loss (using the Finlay-Clay method) and conclude that the cavity loss (excluding the output coupling loss) is roughly the same for all of the Er:YAG rods and is roughly accounted for by the re-absorption loss. It is difficult to apply the Finlay-Clay method to our results with any accuracy, but we estimate that the passive rod losses (including losses due to imperfect antireflection coatings) are <1% and hence in-line with our expectations.

(b) An increase in three-level character due to increased thermal loading density in the rods with higher Er concentrations would contribute to an increase in threshold pump power and a decrease in the slope efficiency with increasing Er concentration. However, calculations supported by experimental results for the effect of rod temperature on performance suggest that this has a very small effect in the power regime in which we are operating.

(c) Energy-transfer upconversion (ETU), via the process $(^4I_{13/2} \rightarrow ^4I_{15/2}) + (^4I_{13/2} \rightarrow ^4I_{9/2})$, is certainly a factor which needs to be taken into consideration and has been the subject of much study in very highly doped Er:YAG crystals because of its importance for operation on the three-micron laser transition: $^4I_{11/2} \rightarrow ^4I_{13/2}$ [16]. However, ETU has not been previously considered to be an issue for operation on the 1646nm regime for low Er doping levels of less than 4at.%. The effect of upconversion on laser performance is considered in detail in the next section.

It is worth noting that in addition to the strong dependence of threshold on Er concentration, there is also a marked decrease in the slope efficiency with increasing Er concentration (see figure 32). Once again the best performance was obtained with the lowest Er doping concentration (0.5at.%). By removing the isolator from our set-up to increase the available pump power and carefully aligning the diffraction grating to ensure that the EYDCFL operated at 1532nm we were able to scale the output power of the 0.5at.% doped Er:YAG laser with a 10% transmitting output coupler to 4.2W for 11.5W of incident pump power (see figure 33) in a TEM_{oo} beam with $M^2 \approx 1.2$. The slope efficiency with respect to absorbed pump power was a little higher (~44%) than we achieved with lower pump powers, but still much lower than we would expect.

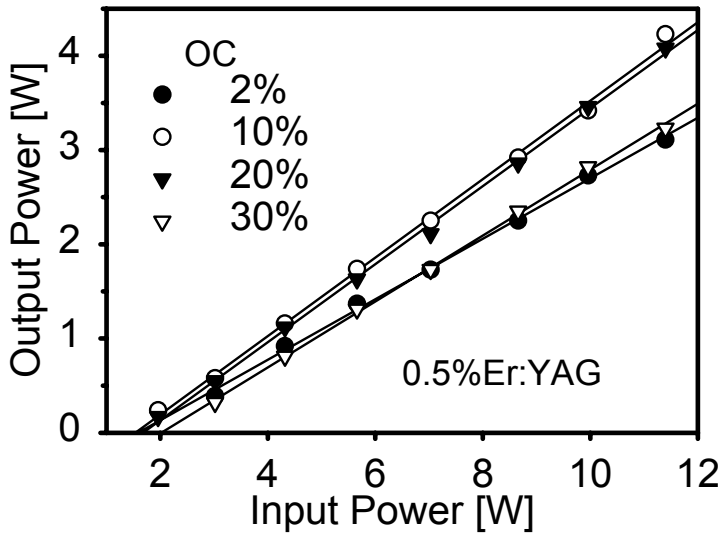

Figure 33: Output power versus incident pump power for 0.5at.% doped Er:YAG laser

4.4 Energy-transfer-upconversion in Er:YAG

We have investigated upconversion in Er:YAG to determine whether it has a significant impact on laser performance for the Er doping levels used in our experiments. For the purpose of this study we have assumed that the population density, N_2, in the upper manifold ($^4I_{13/2}$) under non-lasing conditions can be described by the following rate equation:

$$\frac{dN_2}{dt} = R_p - \frac{N_2}{\tau_f} - \alpha N_2^2 \tag{5}$$

where R_p is the pump rate and α is the upconversion rate parameter for the process ($^4I_{13/2} \rightarrow {}^4I_{15/2}$) and ($^4I_{13/2} \rightarrow {}^4I_{9/2}$). α can be determined from fluorescence decay measurements via the approach that described in ref. 17. The experimental set-up we employed for measuring the upconversion parameter is shown in figure 34. Pump light at 1532nm was provided by the EYDCFL described in section 3.5. The output from the EYDCFL was collimated by a 50mm focal length lens and then focused to a small beam size with the aid of a second 50mm focal

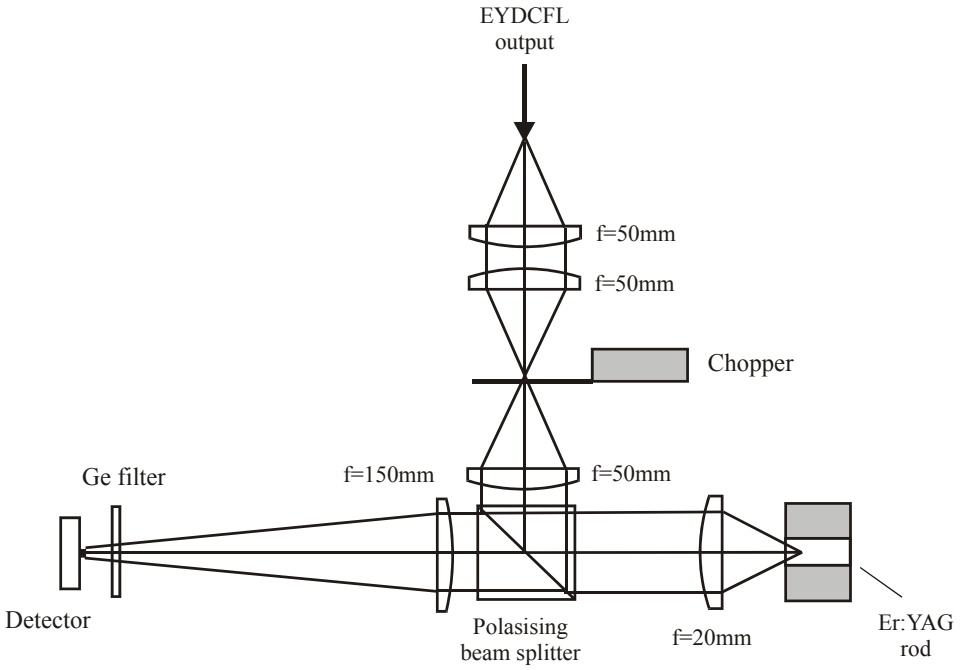

Figure 34: Experimental set-up used for studying upconversion in Er:YAG

length lens. An mechanical chopper was positioned at the pump beam waist to act as a 'fast' shutter for the pump light with a switching speed of <100μs. The pump beam was then re-collimated by another 50mm focal length lens and incident on a polarizing beam-splitter. The polarized pump light reflected from the beam-splitter was then focused to a beam radius of

~90μm in the Er:YAG rod under investigation with the aid of a 20mm focal length lens. For these experiments it is very important that the fluorescence is only detected from the centre of the pumped region where there is high population inversion density. Also, to avoid any misleading results caused by re-absorption, the fluorescence light detected should not propagate through unpumped regions in the sample. Both of these conditions can be fulfilled if the fluorescence is collected with the same lens used for focusing the pump, as is the case in our set-up. The fluorescence transmitted by the beam-splitter was then focused on to an InGaAs detector with the aid of a 150mm focal length lens. The active area of the detector area was only ~1mm^2 and hence was appreciably smaller than the fluorescence spot. In this way only the fluorescence from the centre of the pumped region was monitored by the detector as required. The beam-splitter serves as an effective means to prevent reflected pump light from reaching the detector. However, as an additional precaution a Germanium filter was placed in front of the detector to completely remove any residual pump light. Fluorescence decay curves were measured Er:YAG rods with 0.25at.%, 0.5at.%, 1.0at.%, 2.0at.% and 4at.% Er^{3+} concentrations at high and low pump intensities. Figure 35 shows typical fluorescence decay curves for the 2at.% doped Er:YAG crystal. It can be seen that at low pump intensities the fluorescence power decays as $\exp(-t/\tau_f)$, where τ_f is the lifetime at low excitation densities and is approximately equal to 7ms (as expected). However, at high pump intensities the rate of day is much more rapid indicating that upconversion would have a strong influence at the corresponding excitation density. Figure 36 shows the fluorescence decay curves for Er:YAG rods of different Er doping levels at high pump intensity ($I_p \approx 5I_{p,sat}$). It can be seen that the decay rate is much more rapid for higher concentrations. However, upconversion appears to have only a very small effect on

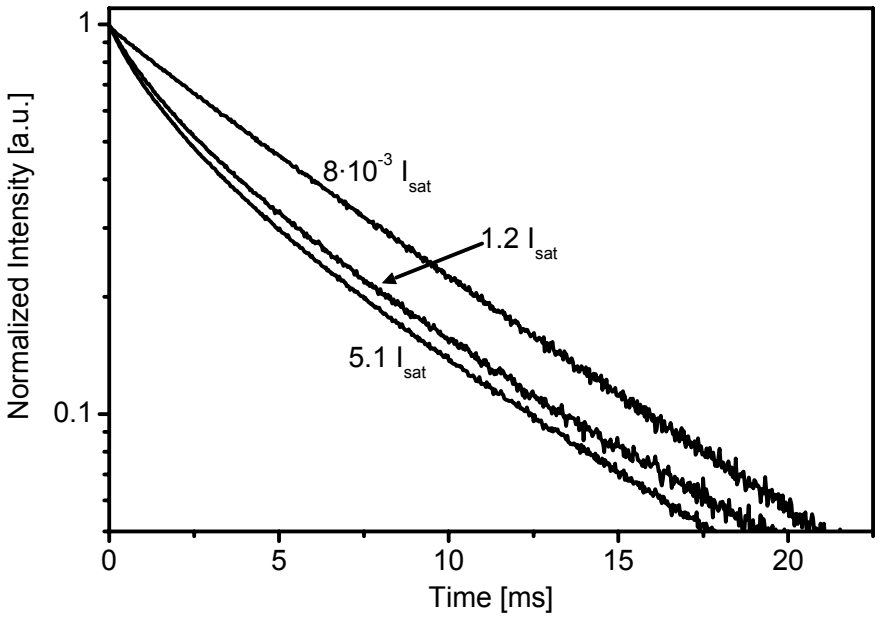

Figure 35: Fluorescence decay of 2% Er^{3+}:YAG at different pump intensities expressed as multiples of the pump saturation intensity.

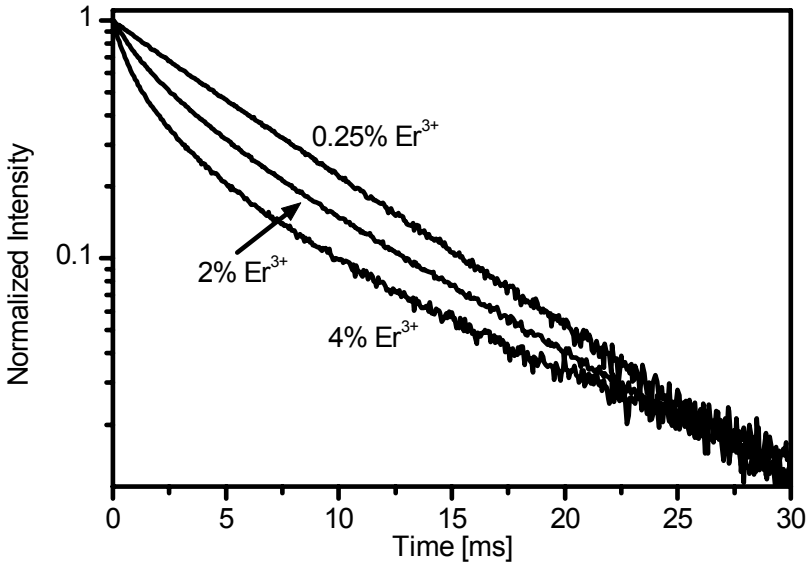

Figure 36: Fluorescence decay curves for Er^{3+}:YAG crystals measured with $I_p \sim 5I_{psat}$.

the decay rate for the 0.25at.% doped Er:YAG rod. The effective lifetime as a function of Er concentration at high pump intensity ($I_p \approx 5I_{p,sat}$) is shown in figure 37. It can be seen that there is a marked reduction in the effective lifetime with increasing Er concentration due to the effect of upconversion. For low pump intensity ($I_p << I_{p,sat}$) the effective lifetime of all Er:YAG crystals is ~7ms. The upconversion parameter, α, can be calculated from the fluorescence day data

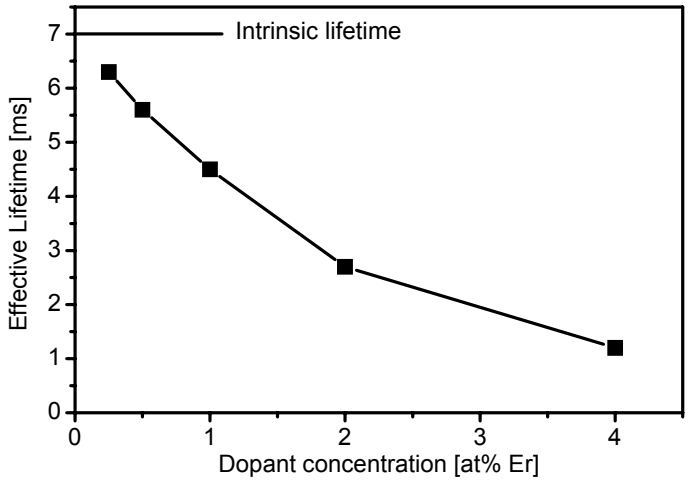

Figure 37: Effective lifetimes of the $^4I_{13/2}$ level in Er^{3+}:YAG at high excitation density

following the procedure outlined in ref.17. The results of this calculation are presented in figure 38. It can be seen that α increases from ~0.6×10^{-18}cm^{3}s^{-1} for the 0.25at.% doped Er:YAG crystal to ~2.7×10^{-18}cm^{3}s^{-1} for the 4at.% doped crystal. For cw lasers the upconversion rate is essentially 'clamped' at threshold, so one obtain a rough idea of whether upconversion is detrimental to performance by simply recalling that threshold pump power:

$$P_{pth} \propto \frac{1}{\tau_{eff}} \tag{6}$$

where τ_{eff} is the effective lifetime given by

$$\frac{1}{\tau_{eff}} = \frac{1}{\tau_f} + \alpha N_{th} \tag{7}$$

where τ_f is the fluorescence lifetime of the upper laser level and N_{th} is the population density in the upper manifold at threshold. Figure 39 shows predicted values for threshold pump power (in

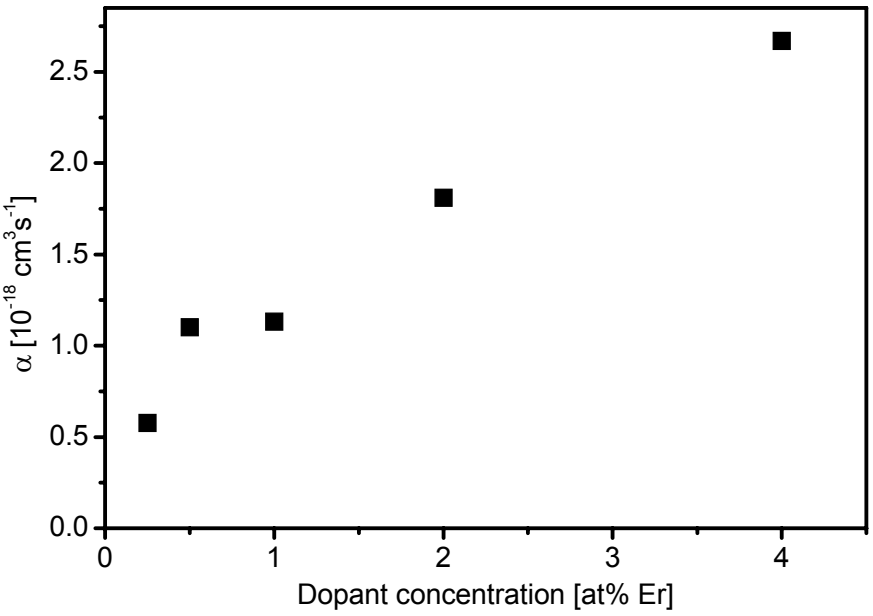

Figure 38: Upconversion parameter (α) for Er^{3+}:YAG versus Er^{3+} concentration

arbitrary units) for our earlier Er:YAG laser design (see section 4.2) as a function of Er concentration taking into account the effect of upconversion. It can be seen that by comparison with the experimental data in figure 31 that the general trends are correctly predicted. However,

it appears that upconversion has a relatively small effect on the cw threshold for doping levels below 2at.% and for cavity losses less than ~10%. Thus upconversion does not account for the strong increase in threshold with increasing Er concentration observed experimentally. Moreover, it cannot explain the decrease in slope efficiency with increasing Er concentration.

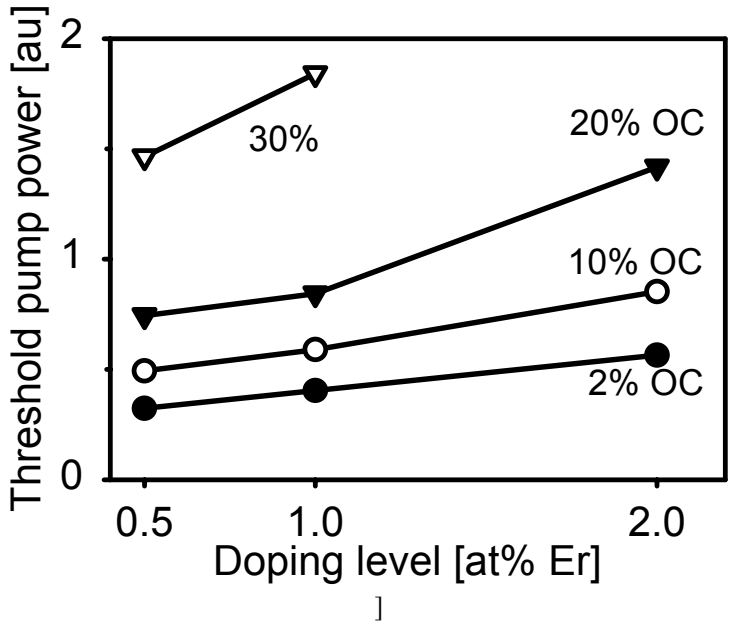

]

Figure 39: Er:YAG threshold (calculated) versus Er concentration

4.5 Summary and future prospects

We have found that the efficiency of Er:YAG lasers operating on the 1646nm is strongly dependent on the Er^{3+} concentration. In comparable laser configurations we observed a dramatic decrease in threshold and increase in slope efficiency by reducing the Er concentration from 2% to 0.5%. This is a very surprising result given that the lasers were all operated in cw mode and had relatively small cavity losses. Energy-transfer-upconversion has been investigated as a possible mechanism for this behaviour. Our results indicate that upconversion does play an important role and should certainly be taken into account when high excitation densities are involved (i.e. in Q-switched lasers or cw lasers with high cavity loss), but does not account for the observed concentration dependence of performance in our laser experiments. There is clearly an additional mechanism (as yet unidentified) which has a very detrimental effect on efficiency and is strongly dependent on Er concentration. Our best Er:YAG laser design to date resulted in a maximum output power of ~4.2W (limited by available pump power) and with a slope efficiency of ~44% from a 0.5at.% doped Er:YAG rod. This slope efficiency is much lower than one would expect from such a laser, and hence motivates further studies aimed at finding an explanation. Reducing the Er^{3+} concentration further may well lead to improved efficiency in

both in cw and pulsed modes of operation, and hence would be advised as a key element of any strategy for further power scaling.

6.0 CONCLUSIONS AND FUTURE WORK

In-band pumping of an Er:YAG laser by a cladding-pumped Er,Yb fiber laser has been investigated. This seemingly simple hybrid laser scheme has proved to be rather more challenging than first thought for several reasons. The relatively short operating wavelength (1532nm) required from the Er,Yb fiber laser makes power-scaling much more difficult than for longer wavelengths, and hence is very demanding on the diode pump and on the core design. However, we believe that with the appropriate design strategy (as outlined in this report) it should be possible to scale to power levels to well in excess of 100W. The most surprising, and perhaps the most concerning, result of our study is the very strong dependence of Er:YAG laser efficiency on Er concentration. Even with a very low Er^{3+} concentration of 0.5at.% the best slope efficiency we could achieve was ~44%, which is much lower than would be expected from this laser system given the very low quantum defect (~7%) and low loss cavity design. Our studies indicate that upconversion does have a detrimental effect on laser performance (even at the low Er concentrations used in our experiments), but does not account for the poor performance. The results suggest that another mechanism (as yet unidentified) is responsible for the decrease in cw lasing efficiency with increasing Er concentration. At the moment all that we can conclude is that further lowering of the Er concentration is a wise move as this will further reduce the effect of upconversion, and may also serve to further reduce the effect of the unidentified loss mechanism to a tolerable level. Further studies are clearly needed to get a better understanding of the factors which influence the efficiency of Er:YAG when operating in cw or pulsed mode to allow a better design strategy to be formulated.

One of the main motivations for this work was to demonstrate efficient Q-switched operation of the Er:YAG laser and assess the potential of this scheme for generating very high pulse energies in the 1.5-1.6μm wavelength regime. Unfortunately, this component of the project has not yet been completed but remains to be an important goal and hence will be the subject of ongoing studies. We anticipate that our preliminary findings will be available within the next few months and will be the subject of an informal written communication to EOARD.

6.0 REFERENCES

1. S. U. Alam, J. Nilsson, P. W. Turner, W. A. Clarkson and A. B. Grudinin, Advanced Solid-State Lasers Technical Digest, (Optical Society of America, Washington, D.C. 2001), p224.
2. J. Nilsson, S. U. Alam, J. A, Alvarez-Chavez, P. W. Turner, W. A. Clarkson and A. B. Grudinin, IEEE J. Quantum Electron., vol.39 (2003), p.987.
3. W. A. Clarkson and D. C. Hanna, Opt. Lett., 21, (1996), 375.
4. D. S. Sumida and D. A. Rockwell. *SPIE Vol. 1627 Solid State Lasers III*, (1992) p273.
5. Le Boulanger, PhD Thesis, University of Caen, France (1998).
6. T. Forster, *Ann. Phys.*, **2**, (1948), p 55.

7. M. Inokuti and F. Hirayama, *J. Chem. Phys.*, vol.1978, (1965), p43.
8. C. Renaud, H.L. Offerhaus, J.A. Alvarez-Chavez, J. Nilsson, W.A. Clarkson, P.W. Turner, D.J. Richardson and A.B. Grudinin, IEEE J. Quantum Electron. 37, 199 (2001)
9. V.G. Shcherbitsky, S. Girard, M. Fromager, R. Moncorgé, N.V. Kuleshov, V.I. Levchenko, V.N. Yakimovich and B. Ferrand, Appl. Phys. B 74, 367 (2002).
10. H. Strange, K. Petermann, G. Huber and E. W. Duczynski, Appl. Phys. B., vol.49 (1989), p.269.
11. Y. E. Young, S. D. Setzler, K. J. Snell, P. A. Budni, T. M. Pollak and E. P. Chicklis, Opt. Lett., vol.29 (2004), p.1075.
12. S. D. Setzler, K. J. Snell, T. M. Pollak, P. A. Budni, Y. E. Young and E. P. Chicklis, Opt. Lett., vol.28 (2003), p.1787.
13. D. Y. Shen, A. Abdolvand, L. J. Cooper and W. A. Clarkson, Appl. Phys. B, vol.79 (2004), p.559.
14. K. Spariosu and M. Birnbaum, IEEE J. Quantum Electron., vol.30 (1994), p.1044.
15. T. Y. Fan and R. L. Byer, IEEE J. Quantum Electron., vol.23 (1987), p.605.
16. S. Georgescu, V. Lupei, A. Lupei, V. I. Zhekov, T. M. Murina and M. I. Studenikin, Opt. Comm., vol.81 (1991), p.186.
17. S. Guy, C. L. Bonner, D. P. Shepherd, D. C. Hanna, A. C. Tropper and B. Ferrand, IEEE J. Quantum Electron., vol.34 (1998), p.900.

7.0 PUBLICATIONS

1. M. Laroche, A. M. Chardon, J. Nilsson, D. P. Shepherd, W. A. Clarkson, "Compact diode-pumped passively Q-switched tunable Er-Yb double-clad fiber laser", Opt. Lett., vol.27 (2002), p.1980.

2. M. Laroche, A. M. Chardon, J. Nilsson, D. P. Shepherd, J. K. Sahu , W. A. Clarkson, S. Girard and R. Moncorge, "Diode-pumped passively Q-switched tunable Er-Yb double-clad fibre laser," CLEO/Europe 2003, paper CL5-5.

3. W. A. Clarkson, "Beam shaping technique for high power diode-stacks," Conference on Lasers and Electro-Optics 2003, paper CThZ2.

4. M. Laroche, W. A. Clarkson, J. K. Sahu , J. Nilsson and Y. Jeong, "High power cladding-pumped tunable Er-Yb fiber laser," Conference on Lasers and Electro-Optics 2003, paper CWO5.

5. P. Jander, J. K. Sahu and W. A. Clarkson, "Efficient Er:YAG lased pumped in-band by an Er/Yb fibre laser", Europhoton Conference on Solid-State and Fiber Coherent Sources, paper ThE3 (2004).

6. M. Laroche, P. Jander, W. A. Clarkson, J. K. Sahu, J. Nilsson and Y. Jeong, "High power cladding-pumped tunable Er,Yb-doped fibre laser", Accepted for publication in Electronics Letters.

7. P. Jander, J. K. Sahu and W. A. Clarkson, "Er^{3+} concentration dependence of energy-transfer-upconversion in Er:YAG", *in preparation.*

8. P. Jander, J. K. Sahu and W. A. Clarkson, "Effect of Er^{3+} concentration on the efficiency of an in-band pumped continuous-wave Er:YAG laser at 1.64μm", *in preparation.*

Appendix A1

Compact diode-pumped passively Q-switched tunable Er–Yb double-clad fiber laser

M. Laroche, A. M. Chardon, J. Nilsson, D. P. Shepherd, and W. A. Clarkson

Optoelectronics Research Centre, University of Southampton, Southampton S017 1BJ, UK

S. Girard and R. Moncorgé

Centre Interdisciplinaire de Recherches Ions Lasers, Unité Mixte de Recherche, 6637 Institut des Sciences de la Matière et du Rayonnement, Commissariat à l'Energie Atomique, Centre National de la Recherche Scientifique, Université de Caen, 6 Boulevard Maréchal Juin, 14050 Caen Cedex, France

Received July 6, 2002

Efficient repetitive passive Q switching of a cladding-pumped Er–Yb fiber laser has been demonstrated by use of an external-cavity configuration containing a Co^{2+}:ZnS crystal as a saturable absorber. Energies of as much as 60 μJ in pulses of durations as short as 3.5 ns (FWHM), corresponding to a peak power of >10 kW, have been generated, and the maximum slope efficiency with respect to the absorbed pump power was 13%. Using a bulk diffraction grating in the Littrow configuration to provide wavelength-selective feedback, we tuned the passively Q-switched fiber laser over 31 nm from 1532 to 1563 nm. The prospects for further improvement in performance are discussed. © 2002 Optical Society of America

OCIS codes: 060.2320, 140.3480, 140.3540, 140.3510, 140.3600.

Over the past decade, progress in the development of efficient diode-pumped, pulsed solid-state lasers operating in the eye-safe wavelength regime near 1.5 μm has been dramatic, fueled by the needs of a variety of scientific, industrial, and defense applications. For some of these applications (e.g., range finding and remote sensing) the requirement for short pulses (a few nanoseconds) has led to the development of compact Er–Yb-doped glass microlasers with active or passive Q switching. By virtue of their very short cavity lengths (typically a few millimeters), these lasers can generate pulses of <8-ns duration and >3-μJ energy.[1] An alternative method for producing pulsed output in the 1.5-μm spectral range is to Q switch an Er–Yb-codoped fiber laser. This approach has the potential attraction that output powers should be scalable to much higher levels without degradation in beam quality by the use of a double-clad fiber design and cladding-pumping.[2] Actively Q-switched single-clad Er and Er–Yb fiber lasers are well established,[3–7] and recently an actively Q-switched cladding-pumped Er–Yb fiber laser was demonstrated.[8] To simplify the resonator design and eliminate the need for external Q-switching electronics, passive Q switching of single-clad Er-doped fiber lasers has also been attempted with a liquefying gallium mirror,[9] a semiconductor saturable absorber,[10] and a Co^{2+}:ZnSe crystal as the saturable absorber.[11] However, the last-named system has shown relatively poor performance, with pulse durations of >1 μs and peak powers of <1 W.

In this Letter we report a cladding-pumped passively Q-switched Er–Yb-codoped fiber laser with a Co^{2+}:ZnS crystal as a saturable absorber, which generates pulses of as much as 60 μJ of energy and a duration of 3.5 ns (FWHM), corresponding to a peak power of >10 kW, and with a maximum slope efficiency with respect to absorbed pump power of 13%. To the best of our knowledge these results show the highest peak power ever recorded in any passively or actively Q-switched Er fiber laser reported to date.

The fiber laser configuration used in our experiments (shown in Fig. 1) consists of ~2 m of Er–Yb-doped circular double-clad fiber (EYDF) and an external cavity that comprises a collimating lens (L_2) of 4.5-mm focal length; a focusing lens (L_3) of focal length 8.6 mm to focus the fiber output into a Co^{2+}:ZnS crystal; a second collimating lens (L_4), of focal length 15 mm, to recollimate the beam; and finally, a diffraction grating, blazed at 1.55 μm with 600 lines/mm, used in the Littrow configuration to provide wavelength-selective feedback. Intracavity focalization into the Co^{2+}:ZnS crystal was found necessary for sufficiently increasing the fluence on the absorber well above saturation. The focal lengths of both L_2 and L_3 were chosen to roughly minimize the mode volume in the Co^{2+}:ZnS crystal to produce a low threshold for passive Q switching, and the crystal was oriented at a small angle with respect to the beam to prevent backreflection into the fiber. The EYDF, fabricated in house by the standard modified chemical-vapor deposition process, had a phosphosilicate core of 11-μm diameter, with Er^{3+} and Yb^{3+} concentrations of 132,000 and 6400 parts in 10^6,

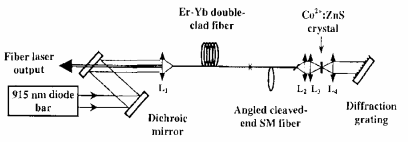

Fig. 1. Schematic of the passively Q-switched fiber laser: SM, single mode.

0146-9592/02/221980-03$15.00/0

respectively, and 0.21 N.A., and it was surrounded by a pure-silica inner cladding of 125-μm diameter. The outer cladding was fabricated from a low-refractive-index ($n = 1.375$) UV-curable polymer, resulting in a high N.A. ($\sim$0.49) for the inner cladding. The EYDF was pumped by a beam-shaped diode bar at 915 nm with 8 W of maximum power. The pump light was coupled into the fiber through a perpendicularly cleaved end facet via an arrangement that comprised two dichroic mirrors, with high reflectivity ($\sim$100%) at 915 nm and high transmission (>95%) at 1.5–1.6 μm, and a gradient-index lens (L_1) of 25-mm focal length with antireflection coatings at the pump and lasing wavelengths. The diffraction grating and a cleaved fiber end facet provided the feedback required for laser oscillation, with the end facet serving as the output coupler. The use of a large-diameter (multimode) core is attractive because it allows for greater energy storage than conventional single-mode core designs,[12] but it obviously has the disadvantage that beam quality is degraded as a result of multimode lasing. To suppress lasing on higher-order modes, a short length ($\sim$400 mm) of standard single-mode fiber with a core diameter of 8 μm was spliced onto the EYDF end adjacent to the external cavity. This fiber is single mode at 1550 nm and has a high-index coating that suppresses light in the cladding. Besides providing for mode selection, its additional advantages are that it reduces amplified spontaneous emission, a few milliwatts in our case, and prevents unabsorbed pump light from damaging the saturable absorber. The end facet of the single-mode fiber was angle cleaved at $\sim 15^{\circ}$ to suppress parasitic lasing between the fiber end facets. When the EYDF was bent into a figure-8 shape (radius of curvature $\approx$2 cm) to improve the overlap of the pump modes with the fiber core, the absorption efficiency of the launched pump power was 95%.

Co^{2+}:ZnS was chosen as the saturable absorber because it has a long metastable lifetime ($\approx$200 μs) and a high ground-state absorption cross section ($\sim 9 \times 10^{-19}$ cm^2), and hence it has a very low saturation fluence[13] (0.1451 J/cm^2 at 1.53 μm). In addition, it has very low nonsaturable losses (<0.1 cm^{-1}) compared with other saturable absorber Q switches, and its absorption spectrum covers a broad wavelength range (1200–1900 nm), making it a suitable candidate for use in tunable Er^{3+} lasers systems operating in the 1.5–1.6-μm spectral region. The Co^{2+}:ZnS crystal used in our experiments was 1 mm thick and had uncoated facets. The small-signal transmission at 1.534 μm was only 9.5%; hence cw lasing was suppressed, even with the high gain value obtained with the EYDF amplifying medium.

Under the operating conditions described above, we found that the threshold for passive Q switching was $\sim$600 mW of absorbed pump power. The average output power and the pulse repetition rate are shown in Fig. 2 as functions of absorbed pump power. The average slope efficiency was $\sim$13% with respect to the absorbed pump power, starting from 600 Hz at threshold and increasing to 6 kHz at the highest pump power (2.75 W absorbed). The pulse train was characterized by relatively stable peak-to-peak intensities (see Fig. 3), and the average pulse-to-pulse temporal jitter recorded over 64 pulses was typically less than $\pm$4%, which is less than for typical passively Q-switched bulk lasers.[14]

One interesting feature of the laser was that the Q-switched pulse duration (approximately 3.5–5 ns) was much shorter than the cavity round-trip time ($\sim$25 ns) and did not vary significantly with pump power. A typical Q-switched pulse (Fig. 3, inset) comprises a main pulse and much lower-power satellite pulses before and after the main pulse. Similarly short pulses were observed previously in Q-switched Er-doped fiber lasers, and various explanations for this behavior, such as the conjunction of Q-switched operation with self-mode locking owing to self-phase modulation[15,16] and the effect of stimulated Brillouin scattering,[17,18] have been proposed. Further research to determine the origin of the short-pulse generation for our passively Q-switched fiber laser is in progress. The pulse energy was measured directly with a calibrated detector to avoid including the effects of amplified spontaneous emission, which can arise when one is determining pulse energy by measurement of the average power and dividing by the pulse repetition frequency. At the maximum pump power, the pulse energy was found to be $\sim$60 μJ, with 75% contained within the main pulse, and corresponds to a peak power of more than 10 kW. This is to our

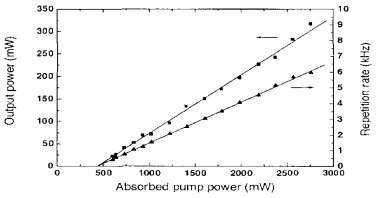

Fig. 2. Average output power (squares) and pulse repetition rate (triangles) versus absorbed pump power.

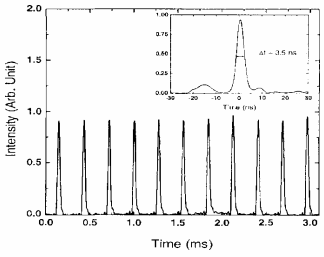

Fig. 3. Typical Q-switched pulse train and (inset) its corresponding temporal pulse shape.

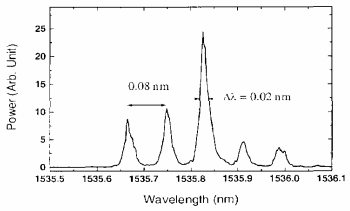

Fig. 4. Output spectrum of the laser on a linear scale. The resolution is 0.002 nm.

knowledge by far the highest peak power reported for any Q-switched Er^{3+} fiber laser oscillator. A further interesting feature of the Q-switched behavior was that the pulse energy did not vary significantly with pump power and was >50 μJ over the full range of pump power used (i.e., 500–2750 mW). A consequence of the generated giant pulse propagating along the fiber is the presence of stimulated Brillouin scattering, which can occur because of the high peak power. The spectrum of the laser is shown in Fig. 4. It was composed of five sharp lines of 0.02-nm width (FWHM), spreading over 0.4 nm and separated by 0.08 nm. Stimulated Brillouin scattering can clearly be identified because this spacing value exactly matches the Brillouin shift in silica near 1550 nm, and this structure can be seen only when a giant pulse is propagating along the fiber. The presence of the diffraction grating also permitted tuning of the output laser signal from 1532 and 1563 nm. Moreover, because of the grating, the output power was 95% vertically polarized.

For comparison, the cw laser performance was also evaluated with the Co^{2+}:ZnS crystal removed from the external cavity while all the other optical components were maintained in place. Under these operating conditions the cw slope efficiency was measured to be 15%, hence only 2% higher than for the passively Q-switched laser. The low value for the cw slope efficiency can easily be explained by the extra resonator losses in the external cavity that are due to the grating, the collimating and focusing lenses, and also the single-mode fiber. It is worth noting that, when the same fiber was employed in a simpler cavity configuration, where feedback for laser oscillation was provided by a high-reflectivity mirror butted to one end of the fiber and by a perpendicularly cleaved fiber end facet, we obtained a maximum slope efficiency of 46% with respect to the absorbed pump power. Thus, by improving the design of the external cavity and using lower-loss components, and by modifying the design of the EYDF, it should be possible to construct a passively Q-switched EYDF laser with much higher efficiency.

In conclusion, we have demonstrated a novel diode-pumped passive Q-switched fiber laser with high-peak-power pulses and broad tunability. This system gives a simple way to obtain more than 10 kW of peak power in a nanosecond pulse, and we believe that, in combination with additional fiber amplifiers, it could offer a route to a compact and reliable tunable millijoule laser. Compact periodically poled $LiNbO_3$ optical parametric oscillator devices pumped by such pulsed fiber sources and emitting in a broad range can also be imaged and could be suitable for many practical applications.[19]

This research is supported by the European Office of Aerospace Research & Development under contract F61775-01-C0008. M. Laroche's e-mail address is mlrl@orc.soton.ac.uk.

References

1. Ph. Thony, B. Ferrand, and E. Molva, in *Advanced Solid State Lasers*, W. R. Bosenberg and M. M. Fejer, eds., Vol. 19 of OSA Trends in Optics and Photonics Series (Optical Society of America, Washington, D.C., 1998), pp. 327.
2. V. Dominic, S. MacCormack, R. Waarts, S. Sanders, S. Bicknese, R. Dohle, E. Wolak, P. S. Yeh, and E. Zucker, Electron. Lett. **35,** 1158 (1999).
3. R. J. Mears, L. Reekie, S. B. Poole, and D. N. Payne, Electron. Lett. **22,** 159 (1986).
4. F. Seguin and T. Oleskevich, Opt. Eng. **32,** 2036 (1993).
5. A. Chandonnet and G. Larose, Opt. Eng. **32,** 2031 (1993).
6. G. P. Lees, A. Hartog, and T. P. Newson, Electron. Lett. **31,** 1836 (1995).
7. H. L. Offerhaus, N. G. Broderick, D. J. Richardson, R. Sammut, J. Caplen, and L. Dong, Opt. Lett. **23,** 1683 (1998).
8. S. U. Alam, P. W. Turner, A. B. Grudinin, and J. Nilsson, in *Conference on Lasers and Electro-Optics (CLEO)*, Vol. 56 of OSA Trends in Optics and Photonics Series (Optical Society of America, Washington, D.C., 2001), pp. 218–219.
9. P. Petropoulos, S. Dhanjal, D. J. Richardson, and N. I. Zheludev, Opt. Commun. **166,** 239 (1999).
10. R. Paschotta, R. Häring, E. Gini, H. Melchior, and U. Keller, Opt. Lett. **24,** 388 (1999).
11. V. N. Filippov, A. N. Starodumov, and A. V. Kir'yanov, Opt. Lett. **26,** 343 (2001).
12. C. C. Renaud, H. L. Offerhaus, J. A. Alvarez-Charvez, J. Nilsson, W. A. Clarkson, P. W. Turner, D. J. Richardson, and A. B. Grudinin, IEEE J. Quantum Electron. **37,** 199 (2001).
13. V. G. Shcherbitsky, S. Girard, M. Fromager, R. Moncorgé, N. V. Kuleshov, V. I. Levchenko, V. N. Yakimovich, and B. Ferrand, Appl. Phys. B **74,** 367 (2002).
14. A. Braud, M. Fromager, J. L. Doualan, S. Girard, R. Moncorgé, M. Thuau, B. Ferrand, and Ph. Thony, Opt. Commun. **183,** 175 (2000).
15. G. P. Lees and T. P. Newson, Electron. Lett. **32,** 332 (1996).
16. P. Myslinski, J. Chrostowski, J. A. K. Koningstein, and J. R. Simpson, Appl. Opt. **32,** 286 (1993).
17. S. V. Chernikov, Y. Zhu, J. R. Taylor, and V. P. Gapontsev, Opt. Lett. **22,** 298 (1997).
18. M. Salhi, A. Hideur, T. Chartier, M. Brunel, G. Martel, C. Ozkul, and F. Sanchez, Opt. Lett. **27,** 1294 (2002).
19. P. E. Briton, D. Taverner, K. Puech, D. J. Richardson, P. G. R. Smith, G. W. Ross, and D. C. Hanna, Opt. Lett. **23,** 582 (1998).

Appendix A2

High power cladding-pumped tunable Er,Yb-doped fibre laser

(Accepted for publication in Electronics Letters)

M. Laroche, P. Jander, W. A. Clarkson, J. K. Sahu, J. Nilsson and Y. Jeong

Optoelectronics Research Centre, University of Southampton, Southampton SO17 1BJ, UK

Corresponding author: W. A. Clarkson, Tel: +44 2380 593776, Fax: +44 2380 593142, E-mail: wac@orc.soton.ac.uk

Abstract: Efficient high-power operation of a tunable erbium-ytterbium co-doped fibre laser end-pumped by two beam-shaped diode-stacks at 940nm is reported. A maximum output power of 30W at 1570nm for 83W of absorbed pump power with operating wavelength tunable from 1562nm to 1627nm was demonstrated.

Introduction: Over the past decade, erbium-doped solid-state lasers operating in the 1.5-1.6μm spectral region have seen rapid development to meet the needs of various applications (e.g. LIDAR and remote monitoring) requiring eyesafe operating wavelengths. For many of these applications, the requirement for high output power is also accompanied by the need for high efficiency and good beam quality, which are often difficult to achieve in conventional 'bulk' Er-doped solid-state lasers due to high thermal loading. Moreover, the combination of relatively narrow emission linewidths and rather low gains that are typical in conventional solid-state lasers restricts the range of operating wavelengths and hence further limits their applicability. Cladding-pumping of Er-Yb doped double clad fibre lasers (EYDFL's) is an alternative route to high power levels in the 1.5μm spectral region [1]. Fibres lasers have the attraction of a geometry which has a high degree of immunity from the effects of thermal loading and hence high efficiencies and good beam quality are achievable [2]. In recent work researchers have demonstrated a cladding-pumped Er-Yb fibre laser with an output power of >100W [3] in a non-tunable resonator configuration. However, a further attraction that fibre lasers offer is the potential for wide wavelength tunability due the broad transition linewidths in glass hosts. In recent work [1], a cladding-pumped Er,Yb-doped fibre laser with wavelength tunable from 1533nm to 1600nm, but with the maximum output power limited to 6.7W was reported. In this letter we describe a cladding-pumped Er-Yb-doped phospho-silicate fibre laser employing a simple diffraction grating feedback cavity with >30W output power at 1568nm and operating wavelength tunable from 1561nm to 1627nm.

Experimental set-up: The Er,Yb co-doped double-clad fibre (EYDF) used in our experiments was pulled from a preform fabricated in-house using the standard chemical vapour deposition and solution doping technique [4]. The resulting fibre had a 24μm diameter phospho-silicate core doped with approximately 0.35% erbium and 1.75% ytterbium (by weight), and a numerical

aperture of 0.21. The inner-cladding was fabricated from pure silica with an outer dimension ~400μm and had a D-shaped cross-section to promote efficient pump absorption. The latter was coated with a low refractive index (n=1.375) UV curable polymer outer-cladding to produce a high numerical aperture waveguide (calculated as 0.49) for the pump, and hence facilitate efficient launch of pump light from high-power, low-brightness diode sources.

The tunable EYDFL (shown in Fig.1) employed a simple external cavity design comprising an 18m length of EYDF, an anti-reflection coated collimating lens of focal length, 25mm, and replica diffraction grating with 600 lines/mm mounted on a copper substrate to facilitate removal of waste heat. The grating was blazed for a wavelength of ~1.65μm with reflectivity ~75% for light polarised parallel to the grooves and ~95% for light polarised in the orthogonal direction, and was aligned in the Littrow configuration to provide wavelength selective feedback and hence the means for adjusting the lasing wavelength. The fibre end facet nearest the external cavity was angle-polished at ~12.5º to the fibre axis to suppress parasitic lasing between the two fibre ends, and the opposite end of the fibre was polished perpendicular to the fibre axis to provide the feedback necessary for lasing. The latter acted as the output coupler with its high transmission (~96.5%) dominating over the external cavity losses. The EYDF was pumped through both fibre end facets by diode-stacks at 940nm. The output beam from each diode-stack was re-formatted, with the aid of a two-mirror beam shaper [5], to roughly equalise the beam propagation factors in orthogonal directions to allow efficient coupling into the fibre. After the beam conditioning optics, each diode-stack module provided a pump power of ~ 65W, of which ~50W was coupled into each end of the EYDF (as shown in Fig.1) with the aid of a 25mm focal length high numerical aperture (GRADIUM) lens and a dichroic mirror to separate the signal light from the pump light. This arrangement, with separate pump focussing and external cavity lenses, has the attraction that it allows independent optimisation of pump launching efficiency and alignment of the external cavity. The effective absorption coefficient for the fibre at 940nm was determined via a cut-back measurement to be ~0.43dB/m and hence a rather long length of fibre ~18m was required for efficient pump absorption (~83%), and to prevent unabsorbed pump from one pump source entering, and possibly damaging, the other pump source.

Experimental results: Under these operating conditions, the EYDFL had a threshold pump power of ~3W (absorbed) and at the maximum available pump power (corresponding to 83W absorbed) yielded 30W of output at 1570nm (see Fig.2). The slope efficiency with respect to absorbed pump power was ~39%, which compares favourably with typical efficiencies obtained in lower power Er,Yb-doped fibre lasers [6]. Furthermore, there was no evidence of lasing on the Yb^{3+} transition at ~1μm, implying efficient energy-transfer from Yb^{3+} to Er^{3+}. The EYDFL operating wavelength was tuned, by adjusting the angle of the diffraction grating, over 66nm from 1562nm to 1627nm (Fig.3). It should be noted that the operating wavelength range is displaced towards the long-wavelength side of the emission line, which peaks at ~1535nm. This is due a combination of increased reabsorption loss at shorter wavelengths and gain saturation due to amplified spontaneous emission at longer wavelengths, which result from the need to use a relatively long fibre for efficient pump absorption. Extension of the tuning range to shorter wavelengths could be achieved by employing diode-stacks with pump wavelength at the absorption peak (~975nm) where the absorption coefficient is approximately six times larger (i.e. 2.6dB/m), which allows a much shorter fibre to be used and/or using an EYDF with reduced Er^{3+}-doping level to reduce the re-absorption loss at short wavelengths and reduce the gain at

longer wavelengths. One interesting feature of the tuning curve (Fig.3) is that there is a pronounced decrease in output power towards longer wavelengths (i.e. from 30W to 19W as the wavelength is tuned from 1568 to 1620nm). The origin of this behaviour is unclear, but could be explained by increased loss at longer wavelengths.

The laser spectrum (see inset of Fig.3) was typically composed of a number of relatively sharp lines of width, 0.03nm (FWHM), spread over a total width of 0.6nm. The output beam had beam quality factor, M^2, of 2.9 due to the slightly multimode nature of the core, which had a V parameter of 10. However, by including a variable size aperture in the feedback cavity, it was possible with careful alignment of the external feedback cavity to improve the beam quality factor to 1.8 with only a 10% reduction in the maximum output power.

Summary: We have demonstrated an efficient cladding-pumped Er,Yb doped phospho-silicate fibre laser with 30W of output power at 1570nm and with operating wavelength tunable from 1562nm to 1627nm utilising a very simple external cavity configuration. This result represents a significant increase in output power by a factor of four over that achieved using a similar EYDFL design and an extension of the tuning range to longer wavelengths. By improving the pump launch efficiency and by optimising the EYDF design and Er^{3+} and Yb^{3+} concentrations it should be possible to achieve a further increase in output power and to extend the tuning range to shorter wavelengths.

Acknowledgments: This worked was funded by EOARD under contract no. F61775-01-C0008.

References

1. J. Nilsson, S.-U. Alam, J. A. Alvarez-Chavez, P. W. Turner, W. A. Clarkson, and A. B. Grudinin, "High-power and tunable operation of erbium-ytterbium co-doped cladding-pumped fiber laser", IEEE J. Quantum Electron. **39**, 987 – 994 (2003)

2. D. C. Brown and H. J. Hoffman, "Thermal, stress and thermo-optic effects in high average power double-clad silica fiber lasers", IEEE J. Quantum Electron., vol.37, pp.208-217, 2001.

3. J. K. Sahu, Y. Jeong, D. J. Richardson and J. Nilsson, "A 103W erbium-ytterbium co-doped large-core fiber laser", Opt. Comm., vol.227, pp.159-163, 2003.

4. G. G. Vienne, J. E. Caplen, L. Dong, J. D. Minelly, J. Nilsson, and D. N. Payne, "Fabrication and characterization of Yb^{3+}:Er^{3+} phosphor-silicate fibers for lasers", J. Lightwave Technol., v. 16, pp. 1990-2001, 1998.

5. W. A. Clarkson and D. C. Hanna, "Two-mirror beam-shaping technique for high-power diode bars", Opt. Lett., v. 21, pp. 375-377, 1996.

6. J. Nilsson, W.A. Clarkson, R. Selvas, J.K. Sahu, P.W. Turner, S.-U. Alam and A.B. Grudinin, “High-power wavelength-tunable cladding-pumped rare-earth-doped silica fiber lasers“, Optical Fiber Technology, vol. 10, pp. 5–30, 2004

Fig. 1

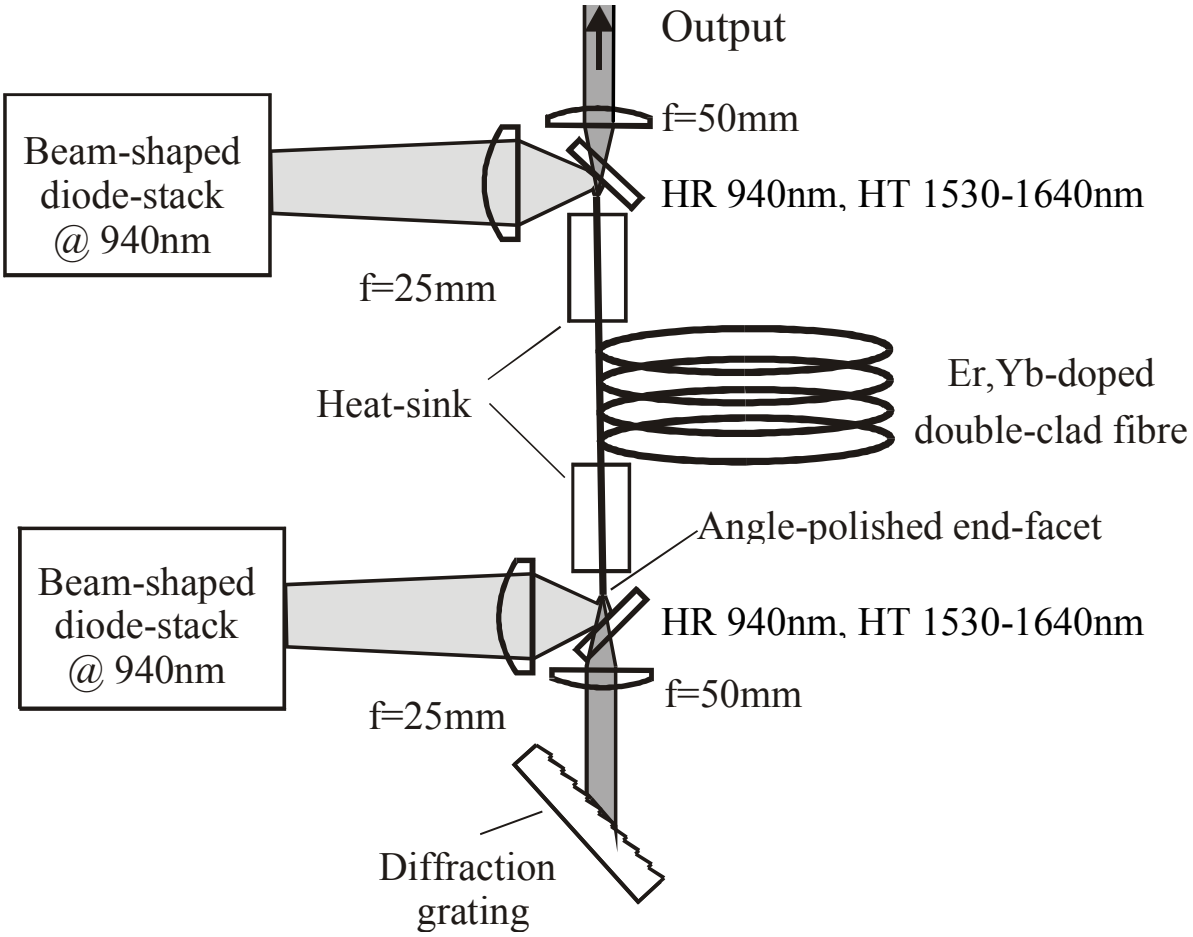

Fig. 1 : Schematic of the Er/Yb fibre laser in a tunable configuration.

Fig. 2

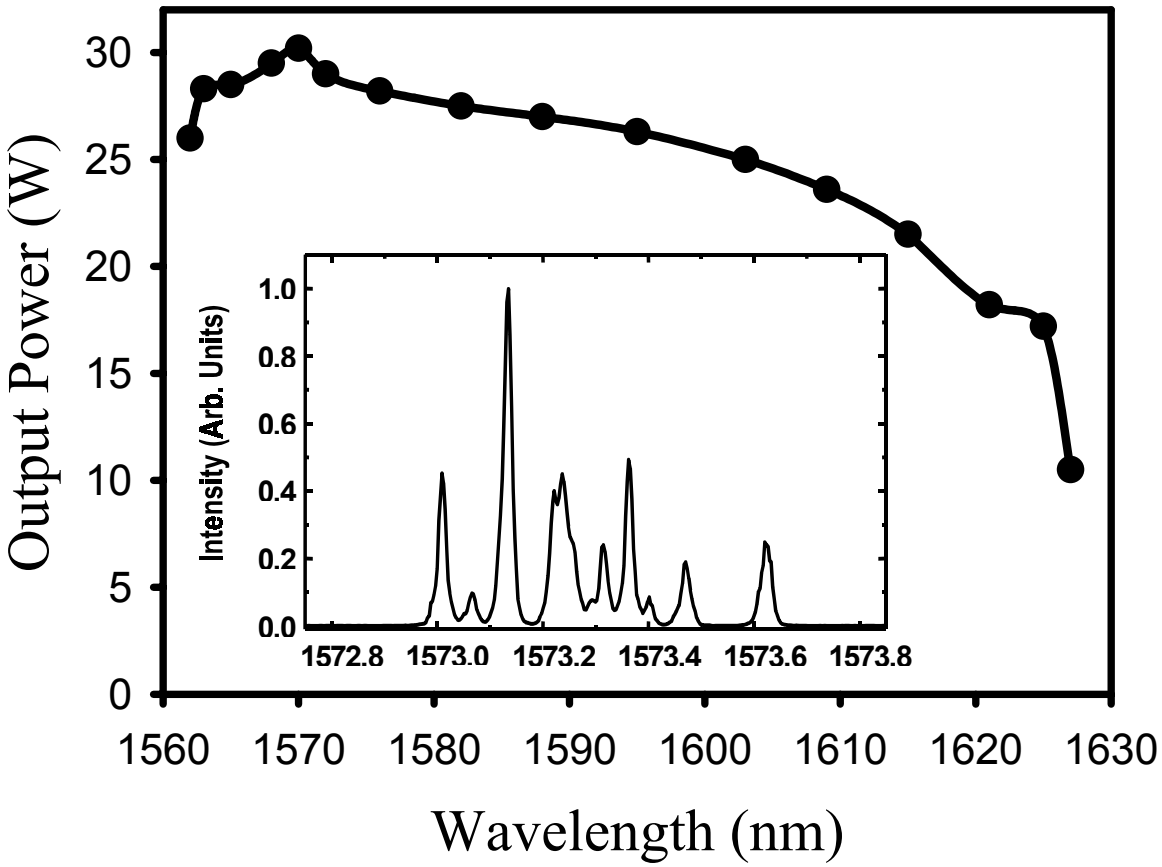

Fig. 2 : Output power versus wavelength, and typical output spectrum of the EYDFL (inset).

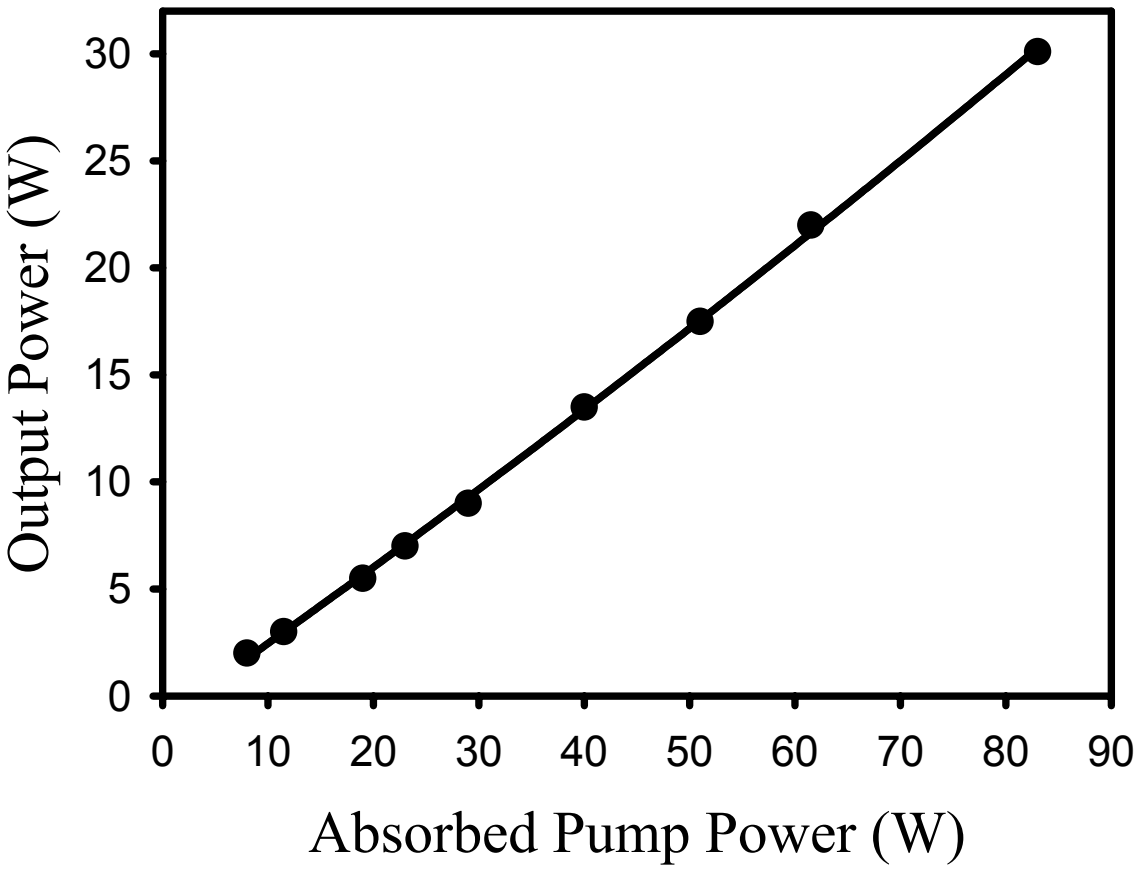

Fig. 3 : Input –output curve of the EYDFL. The slope efficiency is ~39%.

"The Contractor, University of Southampton" hereby declares that, to the best of its knowledge and belief, the technical data delivered herewith under Contract No. F61775-01-C0011 is complete, accurate, and complies with all requirements of the contract.

DATE: 12/10/04
Name and Title of Authorized Official:

Professor W. A. Clarkson

"I certify that there were no subject inventions to declare as defined in FAR 52.227-13, during the performance of this contract."

DATE: 12/10/04
Name and Title of Authorized Official:

Professor W. A. Clarkson